

## Supporting Information

for

### The Bridge towards a more stable and active Side-on-Peroxido ( $\text{Cu}_2^{\text{II}}(\mu\text{-}\eta^2\text{:}\eta^2\text{-O}_2)$ ) complex as a Tyrosinase Model System

Rosalie Dalhoff,<sup>#,a</sup> Regina Schmidt,<sup>#,a</sup> Lena Steeb<sup>a</sup>, Kristina Rabatinova<sup>a</sup>, Matthias Witte<sup>a</sup>, Simon Teeuwen<sup>a</sup>, Salim Benjama<sup>a</sup>,<sup>a</sup> Henrika Hüppe<sup>a</sup>, Alexander Hoffmann<sup>a</sup> and Sonja Herres-Pawlis<sup>\*,a</sup>

## Contents

Supporting Information.....	1
General remarks.....	3
Chemicals.....	4
Experimental.....	5
Analytics.....	5
NMR Nuclear magnetic resonance.....	5
UV/Vis Spectroscopy.....	5
Low temperature stopped-flow UV/Vis spectroscopy.....	5
Mass spectrometry.....	5
Resonance Raman Spectroscopy.....	5
IR Spectroscopy.....	6
Cyclic voltammetric measurements.....	6
Single crystal X-ray diffraction analysis.....	6
DFT calculations.....	7
Synthesis and Characterization.....	7
1,2-Bis(6-bromopyridin-2-yl)ethane.....	7
6,6-(Ethane-1,2-diyl)dipicolinaldehyde.....	8
1,2-Bis(6-(bis(3- <i>tert</i> -butyl)-1H-pyrazol-1-yl)methyl)pyridine-2-yl)ethane <b>L1</b> .....	9
1,2-Bis(6-(di(1H-pyrazol-1-yl)methyl)pyridine-2-yl)ethane <b>L2</b> .....	10
Synthesis of tetra- <i>tert</i> -butylferrocene.....	11
Synthesis of octamethylferrocene.....	11
Complex syntheses.....	13
[ $\text{Cu}_2\{\text{HC}(3\text{-}^t\text{BuPz})_2(\text{CH}_2\text{Py})\}_2\text{Cl}_2$ ] <b>C1</b> .....	13
[ $\text{Cu}_2\{\text{HC}(3\text{-}^t\text{BuPz})_2(\text{CH}_2\text{Py})\}_2\text{Br}_2$ ] <b>C2</b> .....	14
[ $\text{Cu}_2\{\text{HC}(3\text{-}^t\text{BuPz})_2(\text{CH}_2\text{Py})\}_2\text{I}_2$ ] <b>C3</b> .....	15

[Cu <sub>2</sub> {HC(3- <i>t</i> BuPz) <sub>2</sub> (CH <sub>2</sub> Py)} <sub>2</sub> ](PF <sub>6</sub> ) <sub>2</sub> <b>C4</b> .....	15
[Cu <sub>2</sub> {HC(3- <i>t</i> BuPz) <sub>2</sub> (CH <sub>2</sub> Py)} <sub>2</sub> ](OTf) <sub>2</sub> <b>C5</b> .....	16
Preparation of the precursor solution [Cu <sub>2</sub> ( <b>L1</b> )] <sup>2+</sup> (SbF <sub>6</sub> <sup>-</sup> ) <sub>2</sub> <b>C6</b> .....	18
[Cu <sub>2</sub> (HC(3- <i>t</i> BuPz) <sub>2</sub> (CH <sub>2</sub> Py)) <sub>2</sub> O <sub>2</sub> ][SbF <sub>6</sub> ] <sub>2</sub> <b>P</b> .....	18
UV/Vis spectroscopic Experiments .....	19
Temperature dependence of the peroxido formation .....	19
Stability of the peroxido towards different bases .....	19
Substrate hydroxylation catalysis.....	19
Ligand recycling .....	19
Characterization of <b>L1</b> .....	20
Molecular structures of C1-C5 in the solid state .....	21
Characterization of <b>P</b> with Density Functional Theory .....	22
UV/Vis spectroscopic Experiments characterizing properties of <b>P</b> .....	24
Temperature dependency of the formation and stability of <b>P</b> .....	24
Solvent Influence on the formation of <b>P</b> .....	26
Stability of <b>P</b> towards water and bases .....	27
Substrate Catalysis .....	29
Ligand Recycling .....	31
CV measurements .....	33
Spectrophotometric Titrations of <b>P</b> .....	37
Titration of <b>P</b> with decamethylferrocene .....	37
Kinetics .....	39
Iodometric experiments .....	40
Crystallographic Data .....	42
Key geometric parameters and energies of reduced Cu <sub>2</sub> O <sub>2</sub> species .....	50
References.....	51

## General remarks

All reactions and operations were performed under inert nitrogen atmosphere with Schlenk technique. Nitrogen (5.0) was dried over  $P_2O_5$ . Pentane, THF, toluene and diethyl ether were dried over sodium with benzophenone as indicator and purified by distillation under inert atmosphere. DCM, acetonitrile and triethylamine were distilled from  $CaH_2$ . Methanol was purified by distillation from magnesium. All chemicals were used as purchased without further purification. Copper salts ( $[Cu(MeCN)_4]PF_6$ ,  $[Cu(MeCN)_4]OTf$ ) were synthesized according to literature procedure by reaction of  $Cu_2O$  (Sigma Aldrich) and the appropriate acid HX (Sigma Aldrich) in acetonitrile and recrystallized at twice with acetonitrile/diethyl ether<sup>1</sup>.  $CuCl$  was synthesized according to a literature procedure.<sup>2</sup> *Tert*-butyl pyrazole was synthesized according to a literature protocol.<sup>3</sup>

Thin layer chromatography sheets were purchased from Machery-Nagel ( $SiO_2$ , layer thickness 0.20 mm, fluorescent indicator). Column chromatography was performed on Geduran<sup>®</sup> Si 60 (40-63  $\mu m$ , Merck).

All NMR, IR and mass data were deposited as original data in the Chemotion repository<sup>4,5</sup> and are published under an Open Access model. The link to the original data is given in the analytical description.

## Chemicals

All used chemicals, their purity and origin are displayed in Table S1.

**Table S1.** Used chemicals with the origin and purity.

chemical	purity	supplier
1,2-dibromoethane	≥ 98%	Fluka
1H-pyrazole	98%	Sigma Aldrich
2-bromo-6-methylpyridine	96%	Acros
acetone	a.r.g	Fisher Chemicals
acetonitrile	≥ 99.5%	Fisher Chemicals
aluminum oxide	MP Biomedicals	
calcium hydrate	93%	Acros
chloroform	99.90%	Fisher Chemicals
chloroform- <i>d</i>	99.80%	Sigma Aldrich
cobalt(II) chloride	(p.a.)	Sigma Aldrich
copper(II) bromide	99%	abcr
copper(II) chloride	97%	Riedel
copper iodide	98%	Fluka
1,4-diazabicyclo[2.2.2]octane (DABCO)	98%	abcr
1,8-Diazabicyclo[5.4.0]undec-7-ene (DBU)	≥ 99%	Fluka
dichloromethane	p.a.	VWR chemicals
decamethylferrocene	97%	Sigma Aldrich
diethylamine	99%	abcr
	≥ 99,5 %, analytical reagent	
diethyl ether	grade	Fisher scientific
diisopropylamine	99%	abcr
dimethylferrocene	98%	abcr
dimethylformamide		Fisher
ethyl acetate	99.8%	Fisher Chemicals
hydrochloric acid	37%	Fisher Chemicals
hexane	p.a.	Fisher Chemicals
Iron(II) chloride	99.50%	Alfa Aesar
lithium tetramethylcyclopentadienide	95%	abcr
methanol	≥ 99.9%	Fisher Chemicals
sodium carbonate	99.50%	Grüssing
sodium sulfate	99.50%	Fisher
sodium hydrate	60% dispersion in mineral oil	Aldrich
<i>n</i> -butyl lithium (2.5 M in hexane)		Aldrich
o-phenylenediamine	> 98%	Fluka
pentane	a.r.g.	Fisher Chemicals
pyridine	99.50%	abcr
silver hexafluoro antimonate	98%	abcr
sodium	99%	AppliChem
sodium iodide	99%	Alfa Aesar
trifluoro acetic acid (TFA)	99%	TCI
tetrahydrofuran	p.a.	Fisher Chemicals
thionyl chloride	99.50%	Acros
triethylamine	99%	abcr

a.r.g. analytical reagent grade, p.a. pro analysis

## Experimental

### Analytcs

#### NMR Nuclear magnetic resonance

$^1\text{H}$ ,  $^{13}\text{C}\{^1\text{H}\}$  NMR spectra were recorded on a Bruker Avance II 400 or a Bruker Avance III HD 400 nuclear resonance spectrometer at 25 °C. Resonances were referenced to the residual proton signals of the deuterated solvent. Chemical shifts were assigned via two-dimensional NMR measurements. For the Bruker Avance III HD 400 the software Topspin (Version 3.5 pl 7) from Bruker and for the Bruker Avance II 400 the software TopSpin (Version 2.1) from Bruker were used for data acquisition. For visualization and examination of the NMR spectra the software MestReNova (Version 12.0.1-20560) from Mestrelab Research was used.

#### UV/Vis Spectroscopy

UV/Vis spectroscopy was carried out on an Agilent Technologies Cary 60 spectrophotometer connected via a Cary 50 fiber optic coupler and combined with a fiber-optic quartz glass immersion probe (Hellma, 1 mm) and a tailored Schlenk cell. Spectra were recorded using the program Cary WinUV Scanning kinetics 5.0.0.999.

#### Low temperature stopped-flow UV/Vis spectroscopy

Low-temperature stopped-flow UV/Vis spectroscopic measurements were performed with a HI-TECH Scientific SF-61SX2 device with a charge-coupled device (CCD) photodiode array detector and a xenon arc lamp as light source. The optical path length of the quartz glass cuvette was 10 mm and the mixing time amounts to 2 ms. The fastest scan rate was 667 spectra per second in a wavelength range of 300 nm to 800 nm. The analyses were carried out with the TgK Scientific program Kinetic Studio 4.0.12.18336 UV/Vis spectra (250–800 nm) were detected with a temporal resolution of 1.5 ms.

#### Mass spectrometry

Electron spray ionization (ESI) high-resolution mass spectra were recorded on an UHR-TOF Bruker Daltonik maXis II or a ThermoFisher Scientific LTQ Orbitrap XL.

The measurements were performed on an UHR-TOF Bruker Daltonik maXis II, an ESI-quadrupole time-of-flight (qToF) mass spectrometer capable of a resolution of at least 80.000 FWHM. Detection was either in positive or in the negative ion mode. The mass spectrometer was calibrated subsequently to every experiment via direct infusion of a L-proline sodium salt solution, which provided a  $m/z$  range of singly charged peaks up to 3000 Da in both ion modes.

For the ThermoFisher Scientific LTQ Orbitrap XL the source voltage was 4.49 kV and the capillary temperature was 299.54 °C. The tube lens voltage was set between 110 and 130 V.

#### Resonance Raman Spectroscopy

Raman spectra were measured with a modular Raman spectrometer from Gilden Photonics. The modular system consists of a sample chamber and two Omni-Lambda7507 monochromators. The detectors used were highly sensitive photomultipliers with a photomultiplier with a range of 185 to 900 nm from Gilden Photonics. The Raman spectrometer was controlled using GPL FluoroSENS

software (Gilden Photonics). A 405 nm diode laser (cw, 25mW) from CrystaLaser (DL405-025-S-O) was used to excite the samples. The measurements were carried out in a Suprasil fluorescence cuvette.

### IR Spectroscopy

FT-IR spectra were also recorded via a Shimadzu IR Tracer 100 using a Csl beam splitter and an ATR unit (Quest model from Specac utilizing a robust monolithic crystalline diamond) in a 2 cm<sup>-1</sup> resolution. For data acquisition, the software LabSolution IR (Version 2.15) from Shimadzu was used.

### Cyclic voltammetric measurements

Cyclic voltammetric measurements were performed at room temperature with a Metrohm Autolab PGSTAT 101 potentiostat with a three-electrode arrangement with a Pt disc working electrode (1 mm diameter), an Ag wire pseudo reference electrode and a glassy-carbon counter electrode under inert conditions. The samples were prepared with a 0.5–1.0 mM concentration of analyte and 0.1 M NBu<sub>4</sub>PF<sub>6</sub> as supporting electrolyte. Ferrocene was added as internal standard after each measurement. All potentials are referenced relative to the Fc/Fc<sup>+</sup> couple. The cyclic voltammograms were measured with sweep rates of 20, 50, 100 and 200 mV s<sup>-1</sup>.

### Single crystal X-ray diffraction analysis

Determination of the crystal structure of the ligand **L1** and the complexes **C1**, **C2**, **C4**, **C5** and **P** was performed using a STOE four circle diffractometer STADIVARI with Euler-geometry and a Dectris Pilatus3 R 200 K Hybrid-Pixel detector. The source of X-ray is a Genix 3D High Flux which generates Cu-irradiation ( $\lambda = 1.54186 \text{ \AA}$  for **L1** and **C1**) or Mo-irradiation ( $\lambda = 0.71073 \text{ \AA}$  for **C2**, **C4**, **C5** and **P**) and the temperature was regulated via an Oxford Cryostream 800 at 100 K. Data was collected using X-Area Pilatus 3-SV 1.31.131.0<sup>6</sup> and integrated with X-Area Integrate 1.71.0.0<sup>7</sup> and X-Area Recipe 1.33.0.0.<sup>8</sup> The absorption correction was performed via Gaussian integration with Stoe X-Red32 and subsequent scaling of reflections using X-Area LANA 1.71.4.0.<sup>9</sup>

Determination of the crystal structure of the complex **C3** [Cu<sub>2</sub>(**L1**)<sub>2</sub>] was performed using a Bruker D8 Goniometer APEX CCD-planar detector with an INCOATEC microsource with Mo-K $\alpha$  radiation ( $\lambda = 0.71073 \text{ \AA}$ ). The temperature was regulated via an Oxford Cryostream 700 at 100 K. Data was collected with SMART, integrated using SAINT and absorption correction occurred via SADABS.<sup>10</sup>

The structures were solved via direct methods (XPREP<sup>11</sup>; SHELXT<sup>12</sup> or SHELXL<sup>13</sup>) and refined against F<sup>2</sup> via the full matrix method of the least squares.<sup>14</sup> All atoms except for the hydrogen atoms were refined anisotropic with thermic parameters while the hydrogen atoms were localized at idealized positions and were refined isotropic.

The single crystal diffraction data for the ligand **L1** and all complexes are presented in Table 4 - Table 6.

In **C1**, **C2**, **C3** and **P** it was not possible to model the disordered solvent molecules (**C1** and **C1**: four molecules methanol in the unit cell, **C3**: four molecules CH<sub>2</sub>Cl<sub>2</sub> per unit cell and **P**: twelve molecules diethyl ether per unit cell) in an adequate manner, and the data set was treated with the SQUEEZE routine as implemented in PLATON.<sup>15,16</sup> **C3** is a twin and the data set was treated with the TwinRotMat routine as implemented in platon.<sup>15,16</sup>

Full crystallographic data has been deposited with the Cambridge Crystallographic Data Centre as supplementary no. CCDC – 2220005 for **L1**, CCDC – 2220006 for **C1**, CCDC – 2220007 for **C2**, CCDC – 2220008 for **C3**, CCDC – 2220009 for **C4**, CCDC – 2220010 for **C5** and CCDC – 2220011 for **P**. Copies of

the data can be obtained free of charge on application to CCDC, 12 Union Road, Cambridge CB2 1EZ, UK (fax: (+44)1223-336-033; e-mail: [deposit@ccdc.cam.ac.uk](mailto:deposit@ccdc.cam.ac.uk)).

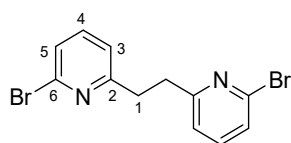
Powder X-ray experiments were performed at ambient conditions on flat samples using a STOE STADI P diffractometer with Debye-Scherrer geometry (Cu-K $\alpha$ 1,  $\lambda$  = 1.54059 Å, STOE image plate detector IP-PSD).

### DFT calculations

All quantum chemical calculations were performed using Gaussian09 revision D.01<sup>17</sup> or Gaussian16 revision B.01<sup>18</sup>. For the calculations, the TPSSh-functional<sup>19–21</sup> and the Ahlrichs triple- $\zeta$  basis set def2-TZVP<sup>22–25</sup> as implemented in Gaussian were used. As empirical dispersion correction, the D3 dispersion with Becke–Johnson damping as implemented in Gaussian was applied.<sup>26–29</sup> Starting geometries for the complexes were obtained via GaussView5.0. The broken symmetry spin state calculations were performed with the opt=stable approach in Gaussian. Optimizations with solvent find no stable minimum or show convergence problems. Thus, only optimizations in the gas phase could be performed. NBO calculations were accomplished using the program suite NBO 7.0 delivering the NBO charges and the charge-transfer energies by second order perturbation theory<sup>30–32</sup>.<sup>[NBO]</sup>

## Synthesis and Characterization

### 1,2-Bis(6-bromopyridin-2-yl)ethane



The synthesis of 1,2-bis(6-bromopyridin-2-yl)ethane was performed according to literature.<sup>33</sup> Diisopropylamine (0.034 mol, 1.0 eq., 4.8 mL) was dissolved in THF (50 mL). At -50 °C *n*-BuLi (0.0390 mol, 1.15 eq., 15.6 mL) was added and the reaction mixture was cooled down to -80 °C. The freshly prepared LDA solution was added dropwise over 20 min to a solution of 2-bromo-6-methylpyridine (0.034 mol, 1.0 eq., 5.9 g) in THF (50 mL) at -80 °C and the reaction mixture was stirred for 2 h at -80 °C. Afterwards, 1,2-dibromoethane (0.034 mol, 1.0 eq., 3.0 mL) was added quickly and the mixture was stirred for 1 h at -78 °C and warmed up to rt. The reaction was terminated by the addition of water (200 mL) and the aqueous layer was extracted with chloroform (3 x 150 mL). The combined organic layers were filtered over Al<sub>2</sub>O<sub>3</sub> giving a clear red solution. After removing the solvent under reduced pressure, the product was obtained as a red crystalline solid (5.60 g, 96.0 %).<sup>33</sup>

<sup>1</sup>H-NMR (400 MHz, CDCl<sub>3</sub>):  $\delta$  = 7.42 (t, <sup>3</sup>*J*<sub>H,H</sub> = 7.8 Hz; 2 H, 4-H(py)), 7.31 (dd, <sup>3</sup>*J*<sub>H,H</sub> = 7.9 Hz, <sup>4</sup>*J*<sub>H,H</sub> = 0.9 Hz, 2 H; 3-H(py)), 7.08 (dd, <sup>3</sup>*J*<sub>H,H</sub> = 7.5 Hz, <sup>4</sup>*J*<sub>H,H</sub> = 0.8 Hz, 2 H; 5-H(py)), 3.20 (s, 4 H; CH<sub>2</sub>(1)) ppm.

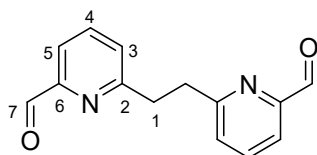
<sup>13</sup>C-NMR (101 MHz, CDCl<sub>3</sub>):  $\delta$  = 162.5 (2-C(py)), 141.8 (6-C(py)), 138.8 (4-C(py)), 125.8 (5-C(py)), 122.1 (3-C(py)), 37.3(1) ppm.

IR (ATR,  $\tilde{\nu}$ ) = 3070 (vw), 3019 (vw), 2965 (vw), 2930 (w), 2841 (w), 1752 (w), 1700 (vs), 1667 (w), 1589 (vs), 1546 (w), 1459 (m), 1362 (m), 1296 (w), 1280 (w), 1236 (w), 1214 (s), 1163 (w), 1076 (w), 1005 (vw), 992 (s), 919 (s), 810 (vs), 774 (vs), 744 (s), 643 (vs), 545 (m), 477 (w)  $\text{cm}^{-1}$ .

HRMS (ESI+, MeOH):  $m/z$  (%) (found): 340.92822 (51.9), 341.93140 (5.6), 342.92621 (100), 343.92932 (11.3), 344.92422 (55.0), 345.92746 (4.4)  $[M+H]^+$ ; (calc.): 340.9283506 (51.4)  $[\text{C}_{12}\text{H}_{11}^{79}\text{Br}_2\text{N}_2]^+$ , 341.9317054 (6.7)  $[\text{C}_{11}^{13}\text{CH}_{11}^{79}\text{Br}_2\text{N}_2]^+$ , 342.9263037 (100)  $[\text{C}_{12}\text{H}_{11}^{79}\text{Br}^{81}\text{BrN}_2]^+$ , 343.9296585 (13.0)  $[\text{C}_{11}^{13}\text{CH}_{11}^{79}\text{Br}^{81}\text{BrN}_2]^+$ , 344.9242568 (48.6)  $[\text{C}_{12}\text{H}_{11}^{81}\text{Br}_2\text{N}_2]^+$ , 335.9276116 (6.3)  $[\text{C}_{11}^{13}\text{CH}_{11}^{81}\text{Br}_2\text{N}_2]^+$ .

Additional information on the NMR spectra of the target compound including original data files is available via the Chemotion Repository: <https://dx.doi.org/10.14272/reaction/SA-FUHFF-UHFFFADPSC-AEZGGXCUYL-UHFFFADPSC-NUHFF-NUHFF-NUHFF-ZZZ>

### 6,6-(Ethane-1,2-diyl)dipicolinaldehyde



Synthesis of 6,6-(ethane-1,2-diyl)dipicolinaldehyde was performed according to literature.<sup>34</sup> 1,2-Bis(6-bromopyridin-2-yl)ethane (0.16 mol, 1.0 eq., 5.5 g) was dissolved in degassed THF (300 mL). At  $-80\text{ }^\circ\text{C}$  *n*-BuLi (0.042 mol, 2.5 eq., 17 mL (2.5 M)) was added dropwise over 5 min and the reaction mixture was stirred at  $-80\text{ }^\circ\text{C}$  for 1 h. A solution of DMF (0.065 mol, 4.0 eq., 5.0 mL) in THF (42 mL) was added over 30 min. The reaction mixture was stirred 20 min at  $-20\text{ }^\circ\text{C}$  and additional 15 h at rt. Afterwards, HCl (2 M, 42 mL) was added, the emulsion was stirred for 30 min and it was concentrated under stirring and reduced pressure. A mixture of DCM (200 mL), water (100 mL) and ice (100 mL) was added and the aqueous layer was neutralized with  $\text{Na}_2\text{CO}_3$  while cooling the flask in an ice bath. The aqueous layer was extracted with DCM (5 x 100 mL) and the combined organic layers were dried over  $\text{Na}_2\text{SO}_4$ . A brown solid crushed out, which was filtered and washed with cold acetonitrile (40 mL) giving a light brown solid (900 mg, 23 %).<sup>34</sup>

$^1\text{H-NMR}$  (400 MHz,  $\text{CDCl}_3$ ):  $\delta$  = 10.06 (s, 2 H; H(7)), 7.81-7.72 (m, 4H; 5-H(py), 4-H(py)), 7.38 (dd,  $^3J_{\text{H,H}} = 7.4$ ,  $^4J_{\text{H,H}} = 1.3$  Hz, 2 H; 3-H(py)), 3.43 (s, 4H,  $\text{CH}_2$ ) ppm.

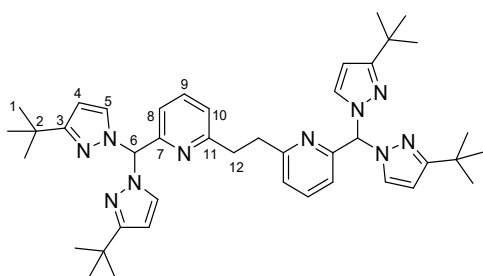
$^{13}\text{C-NMR}$  (101 MHz,  $\text{CDCl}_3$ ):  $\delta$  = 193.9 (CHO), 161.8 (2-C(py)), 152.7 (6-C(py)), 137.4 (4-C(py)), 127.6 (3-C(py)), 119.6 (5-C(py)), 37.2 ( $\text{CH}_2$ ) ppm.

IR (ATR,  $\tilde{\nu}$ ) = 2933 (vw), 2842 (w), 1700 (vs), 1664 (w), 1590 (vs), 1459 (m), 1447 (w), 1433 (vw), 1362 (m), 1297 (w), 1280 (w), 1236 (w), 1214 (s), 1164 (w), 1135 (vw), 1077 (w), 1056 (vw), 1006 (vw), 992 (s), 927 (w), 919 (s), 901 (vw), 810 (vs), 774 (vs), 744 (vs), 643 (vs), 588 (w), 545 (m), 476 (w)  $\text{cm}^{-1}$ .

HRMS (ESI<sup>+</sup>, MeOH): *m/z* (%) (found): 241.09720 (100), 242.10042 (14.3) [*M*+H]<sup>+</sup>; (calc.): 241.0971541 (100) [C<sub>14</sub>H<sub>13</sub>N<sub>2</sub>O<sub>2</sub>]<sup>+</sup>, 242.1005089 (15.1) C<sub>13</sub><sup>13</sup>CH<sub>13</sub>N<sub>2</sub>O<sub>2</sub><sup>+</sup>.

Additional information on the NMR spectra of the target compound including original data files is available via the Chemotion Repository: <https://dx.doi.org/10.14272/reaction/SA-FUHFF-UHFFFADPSC-ZLWCJIJDQB-UHFFFADPSC-NUHFF-NUHFF-NUHFF-ZZZ>

### 1,2-Bis(6-(bis(3-*tert*-butyl)-1H-pyrazol-1-yl)methyl)pyridine-2-yl)ethane L1



The synthesis was performed in accordance to general procedure for bis(pyrazolyl)methanes.<sup>35</sup> NaH (0.016 mol, 4.0 eq., 0.39 g) was suspended in degassed THF (17 mL). At 0 °C 3-*tert*-butyl pyrazole (0.017 mol, 4.2 eq., 2.1 g) was added and the resulting reaction mixture was stirred at 0 °C for 30 min. Afterwards, SOCl<sub>2</sub> (0.008 mol, 2 eq., 0.6 mL) was added dropwise over 10 min at 0 °C. The reaction mixture was stirred for 30 min at 0 °C and for additional 30 min at rt. 6,6-(Ethane-1,2-diyl)dipicolinaldehyde (0.0040 mol, 1.0 eq., 1.0 g) and catalytic amounts of CoCl<sub>2</sub> were added and the green reaction mixture was refluxed for 41 h. After cooling down to rt, water (30 mL) and Et<sub>2</sub>O (30 mL) were added, and the biphasic system was stirred for 3.5 h. The aqueous phase was extracted with Et<sub>2</sub>O (3 x 30 mL) and the combined organic layers were washed with water and brine and dried over Na<sub>2</sub>SO<sub>4</sub>. The solvent was removed under reduced pressure and the resulting brown oil was purified via column chromatography (hexane : ethyl acetate (4:1), *r<sub>f</sub>* = 0.38). A colorless solid was obtained which was dissolved in warm ethyl acetate. After some days the product crystallizes as colorless crystals (1.13 g, 39.0 %).<sup>35</sup>

<sup>1</sup>H-NMR (400 MHz, CDCl<sub>3</sub>): δ = 7.55 (s, 2 H; CH), 7.45 (t, <sup>3</sup>*J*<sub>H,H</sub> = 7.8 Hz, 2 H; 9-H(py)), 7.28 (d, <sup>3</sup>*J*<sub>H,H</sub> = 2.2 Hz, 4 H; 5-H(pz)), 6.90 (d, <sup>3</sup>*J*<sub>H,H</sub> = 8.1 Hz, 2H; 10-H(py)), 6.69 (d, <sup>3</sup>*J*<sub>H,H</sub> = 7.8 Hz, 2 H; 8-H(py)), 6.11 (d, <sup>3</sup>*J*<sub>H,H</sub> = 2.4 Hz, 4 H; 4-H(pz)), 3.15 (s, 4 H; CH<sub>2</sub>), 1.28 (s, 36 H; H(<sup>*t*</sup>Bu)) ppm.

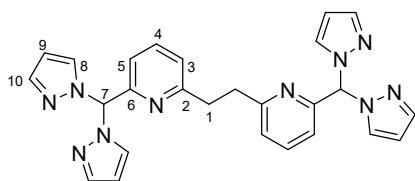
<sup>13</sup>C-NMR (101 MHz, CDCl<sub>3</sub>): δ = 162.9 (3-C(pz)), 161.0 (11-C(py)), 155.1 (7-C(py)), 137.1 (9-C(py)), 129.9 (4-C(pz)), 123.4 (10-C(py)), 119.6 (8-C(py)), 102.7 (2-C(pz)), 78.5 (CH), 36.9 (CH<sub>2</sub>), 32.3 (C<sup>*tert*</sup>), 30.7 (C(<sup>*t*</sup>Bu)) ppm.

IR (ATR,  $\tilde{\nu}$ ) = 3985 (vw), 2960 (w), 1594 (w), 1575 (w), 1533 (vw), 1516 (w), 1458 (m), 1403 (w), 1362 (w), 1357 (w), 1325 (w), 1248 (vs), 1227 (w), 1206 (w), 1156 (w), 1098 (vw), 1054 (s), 1049 (s), 993 (w), 983 (vw), 979 (vw), 865 (vw), 829 (w), 819 (w), 795 (m), 781 (w), 767 (vs), 759 (vs), 741 (vw), 724 (m), 664 (vw), 655 (w), 556 (vw), 443 (w) cm<sup>-1</sup>.

HRMS (ESI+, MeOH):  $m/z$  (%) (found): 701.47650 (100), 702.47913 (48.0), 703.48285 (9.6)  $[M+H]^+$ , (calc.): 701.4762183 (100)  $[C_{42}H_{57}N_{10}]^+$ , 702.4795732 (45.4)  $[C_{41}^{13}CH_{57}N_{10}]^+$ , 703.4829280 (10.0)  $[C_{40}^{13}C_2H_{57}N_{10}]^+$ .

Additional information on the NMR spectra of the target compound including original data files is available via the Chemotion Repository: <https://dx.doi.org/10.14272/reaction/SA-FUHFF-UHFFFADPSC-CTVCMXWPOR-UHFFFADPSC-NUHFF-NUHFF-NUHFF-ZZZ>

## 1,2-Bis(6-(di(1*H*-pyrazol-1-yl)methyl)pyridine-2-yl)ethane L2



The synthesis was performed in accordance to general procedure for bis(pyrazolyl)methanes.<sup>35</sup> NaH (3.25 mmol, 3.90 eq., 77.9 mg) was suspended in degassed THF (5 mL) and 1*H*-pyrazole (3.41 mmol, 4.10 eq., 0.232 g) was added. After stirring for 30 min at 0 °C, SOCl<sub>2</sub> (1.65 mmol, 2.00 eq., 0.120 mL) was added dropwise and the solution was stirred for 30 min at 0 °C and for additional 30 min at ambient temperature. 1,2-bis(2-formyl-6pyridinyl)ethane (0.830 mmol, 1.00 eq., 200 mg) and catalytic amounts of CoCl<sub>2</sub> were added and the reaction mixture was heated to reflux for 42 h. The reaction was terminated by the addition of water (6 mL) and Et<sub>2</sub>O (6 mL) and the resulting biphasic system was stirred for 45 h. The aqueous phase was extracted with Et<sub>2</sub>O (4 x 8 mL) and the combined organic layers were washed with water and brine and dried over MgSO<sub>4</sub>. After purification via column chromatography (EtOAc), the product was obtained as a light brown solid (0.030 mmol, 13.5 mg, 4.0 %).<sup>35</sup>

<sup>1</sup>H-NMR (400 MHz, CDCl<sub>3</sub>):  $\delta$  = 7.68 (s, 2 H; CH), 7.61 (dd, <sup>3</sup> $J_{H,H}$  = 1.8 Hz, <sup>4</sup> $J_{H,H}$  = 0.6 Hz, 4H; 8-H(pz)), 7.56-7.51 (m, 6 H; 4-H(py), 10-H(pz)), 7.00 (dd, <sup>3</sup> $J_{H,H}$  = 7.9 Hz, <sup>4</sup> $J_{H,H}$  = 0.9 Hz, 2 H; 3-H(py)), 6.88 (d, <sup>3</sup> $J_{H,H}$  = 7.7 Hz, 2 H; 5-H(py)), 6.31 (dd, <sup>3</sup> $J_{H,H}$  = 2.5 Hz, <sup>4</sup> $J_{H,H}$  = 1.8 Hz, 4 H; 2-H(pz)), 3.19 (s, 4 H; CH<sub>2</sub>) ppm.

<sup>13</sup>C-NMR (101 MHz, CDCl<sub>3</sub>):  $\delta$  = 161.2 (2-C(py)), 153.9 (6-C(py)), 140.7 (10-C(pz)), 137.6 (6-C(py)), 130.0 (8-C(pz)), 123.8 (5-C(py)), 119.9 (3-C(py)), 106.6 (9-C(pz)), 78.7 (CH), 36.6 (CH<sub>2</sub>) ppm.

IR (ATR,  $\tilde{\nu}$ ) = 1707 (w), 1593 (m), 1575 (w), 1513 (w), 1458 (m), 1431 (w), 1391 (m), 1368 (w), 1356 (w), 1320 (w), 1315 (w), 1304 (w), 1288 (w), 1261 (w), 1246 (vw), 1206 (w), 1174 (vw), 1160 (w), 1082 (s), 1045 (s), 997 (w), 967 (w), 956 (w), 913 (w), 881 (vw), 821 (m), 775 (vs), 746 (vs), 670 (w), 666 (w), 649 (w), 641 (vs), 613 (w), 607 (w), 554 (w) cm<sup>-1</sup>.

HRMS (ESI+, MeOH):  $m/z$  (%) (found): 499.2093 (100), 500.2116 (30.6), 501.2192 (3.5)  $[M+Na]^+$ ; (calc.): 499.2077619 (100)  $[C_{26}H_{24}N_{10}Na]^+$ , 500.2111168 (28.1)  $[C_{25}^{13}CH_{24}N_{10}Na]^+$ , 501.2135 (3.8)  $[C_{24}^{13}C_2H_{24}N_{10}Na]^+$ .

Additional information on the NMR spectra of the target compound including original data files is available via the Chemotion Repository: <https://dx.doi.org/10.14272/reaction/SA-FUHFF-UHFFFADPSC-ZPJVIPQPOY-UHFFFADPSC-NUHFF-NUHFF-NUHFF-ZZZ>

### Synthesis of tetra-*tert*-butylferrocene

The synthesis was performed according to a modified literature protocol.<sup>36,37</sup> 1,3-Di-*tert*-butyl cyclopentadiene (9.37 mmol, 2.0 eq., 1.670 g, 2.0 mL) was dissolved in THF (20 mL) and cooled to -80 °C, then *n*-butyl lithium (9.4 mmol, 2.0 eq., 2.5 M in hexane, 3.7 mL) was added dropwise. After stirring the solution for 30 min at -80 °C, FeCl<sub>2</sub> (4.68 mmol, 1.00 eq., 0.593 g) was added and the solution was warmed to rt. After stirring for 1 h the reaction was quenched with ice-cold water (70 mL). THF was evaporated under reduced pressure and the aqueous phase was extracted with *n*-hexane (3x 100 mL). The combined organic layers were dried over MgSO<sub>4</sub>, filtered and the solvent was evaporated under reduced pressure. The raw product was dried and then sublimated under static reduced pressure at 120 °C to obtain the product as orange crystalline solid (2.68 mmol, 1.10 g, 57.0 %).

<sup>1</sup>H-NMR (400 MHz, CDCl<sub>3</sub>): δ = 3.94 (br, 6 H, CH(cy)), 1.20 (br, 36 H, CH(CH<sub>3</sub>)) ppm.

IR (ATR,  $\tilde{\nu}$ ) = 2957 (vs), 2930 (m), 2899 (m), 2865 (m), 1484 (m), 1460 (m), 1388 (m), 1361 (s), 1298 (m), 1251 (s), 1231 (w), 1199 (m), 1199 (m), 1164 (w), 1135 (w), 1048 (m), 1023 (w), 940 (m), 911 (m), 842 (vs), 810 (m), 678 (m), 657 (m), 618 (m), 513 (s), 498 (m) cm<sup>-1</sup>.

HRMS (ESI+, MeOH): *m/z* (%) (found): 408.26730 (6.3), 409.27055 (1.9), 410.26202 (100), 411.26501 (30.6), 412.26811 (4.4) [*M*<sup>+</sup>]; (calc.): 408.267718 (6.67) [C<sub>26</sub>H<sub>42</sub><sup>54</sup>Fe]<sup>+</sup>, 409.271072 (1.79) [C<sub>25</sub><sup>13</sup>C<sub>1</sub>H<sub>42</sub><sup>54</sup>Fe]<sup>+</sup>, 410.263045 (100) [C<sub>26</sub>H<sub>42</sub><sup>56</sup>Fe]<sup>+</sup>, 411.266399 (28.1) [C<sub>25</sub><sup>13</sup>CH<sub>42</sub><sup>56</sup>Fe]<sup>+</sup>, 412.269754 (3.80) [C<sub>24</sub><sup>13</sup>C<sub>2</sub>H<sub>42</sub><sup>56</sup>Fe]<sup>+</sup>.

Additional information on the NMR spectra of the target compound including original data files is available via the Chemotion Repository: <https://dx.doi.org/10.14272/reaction/SA-FUHFF-UHFFFADPSC-GDNSZQMZEW-UHFFFADPSC-NUHFF-NUHFF-NUHFF-ZZZ>

### Synthesis of octamethylferrocene

The synthesis was performed according to a modified literature protocol.<sup>36,37</sup> Lithium tetra-*tert*-butyl cyclopentadienide (0.600 g, 4.68 mmol, 2.00 eq.) was dissolved in THF and FeCl<sub>2</sub> (0.23 mg, 2,3 mmol, 1.0 eq.) was added. After stirring for 1h at rt the reaction mixture was heated to reflux for 8 h. The reaction was quenched by adding ice-cold water (35 mL). THF was removed under reduced pressure and the aqueous phase was extracted with *n*-hexane (3x 50 mL). The combined organic layers were dried over MgSO<sub>4</sub>, filtered and dried under reduced pressure. The raw product was purified by sublimation under static reduced pressure at 120 °C to receive the product as orange crystalline solid (0.511 g, 1.72 mmol, 73.0 %).

<sup>1</sup>H-NMR (400 MHz, CDCl<sub>3</sub>): δ = 3.64 (br, 2 H, CH(cy)), 1.39 (br, 24 H, CH(CH<sub>3</sub>)) ppm.

IR (ATR,  $\tilde{\nu}$ ) = 3065 (w), 2965 (m), 2943 (m), 2897 (m), 2859 (m), 1637 (w), 1487 (w), 1424 (w), 1418 (w), 1378 (s), 1330 (w), 1141 (w), 1071 (w), 1027 (s), 972 (w), 925 (w), 820 (vs), 783 (w), 690 (w), 569 (w), 503 (m), 459 (m)  $\text{cm}^{-1}$ .

HRMS (ESI+, MeOH):  $m/z$  (%) (found): 296.14302 (6.3), 298.13785 (100) 299.14087 (21.9), 300.14436 (1.9)  $[M]^+$ ; (calc.): 296.142517 (6.37)  $[\text{C}_{18}\text{H}_{26}^{54}\text{Fe}]^+$ , 298.137844 (100)  $[\text{C}_{18}\text{H}_{26}^{56}\text{Fe}]^+$ , (19.5)  $[\text{C}_{17}^{13}\text{C}_1\text{H}_{26}^{56}\text{Fe}]^+$ , 300.144554 (1.79)  $[\text{C}_{16}^{13}\text{C}_2\text{H}_{26}^{56}\text{Fe}]^+$ .

Additional information on the NMR spectra of the target compound including original data files is available via the Chemotion Repository: <https://dx.doi.org/10.14272/reaction/SA-FUHFF-UHFFFADPSC-VSUTUDRPAA-UHFFFADPSC-NUHFF-NUHFF-NUHFF-ZZZ>

## Complex syntheses

### $[\text{Cu}_2\{\text{HC}(3\text{-}^t\text{BuPz})_2(\text{CH}_2\text{Py})\}_2\text{Cl}_2]$ **C1**

A solution of ligand **L1** (0.025 mmol, 1 eq., 17.5 mg) dissolved in MeOH was added dropwise to a solution of  $\text{CuCl}_2$  (0.050 mmol, 2.0 eq., 6.7 mg) in MeOH (1 mL). The solution was stirred for 1 h at rt and then filtered through a Whatman® filter. The clear yellow solution was layered with pentane. After 3 days yellow crystals suitable for XRD analysis were received.

IR (ATR,  $\tilde{\nu}$ ) = 3131 (vw), 3110 (w), 2963 (m), 2928 (w), 2904 (w), 2864 (w), 1601 (w), 1571 (w), 1518 (m), 1482 (w), 1461 (s), 1417 (w), 1364 (w), 1346 (w), 1286 (vw), 1236 (s), 1216 (w), 1168 (w), 1156 (w), 1134 (w), 1059 (m), 1036 (w), 1013 (w), 1007 (w), 995 (w), 978 (w), 965 (w), 844 (w), 826 (w), 773 (vs), 748 (w), 738 (vw), 728 (w), 663 (s), 642 (w), 606 (w), 584 (w), 505 (w), 495 (w), 466 (w), 440 (w), 428 (w), 406 (w), 401 (w)  $\text{cm}^{-1}$ .

HRMS (ESI+, MeOH):  $m/z$  (%) (found): 861.29799 (78.1), 862.30118 (36.3) 863.29626 (100) 864.29889 (44.7), 865.29382 (36.3), 866.29646 (15.3), 867.228844 (3.1)  $[\text{M}-\text{Cl}]^+$ ; (calc.): 861.296441 (100)  $[\text{C}_{42}\text{H}_{56}^{35}\text{Cl}^{63}\text{Cu}_2\text{N}_{10}]^+$ , 862.299796 (45.4)  $[\text{C}_{41}^{13}\text{CH}_{56}^{35}\text{Cl}^{63}\text{Cu}_2\text{N}_{10}]^+$ , 863.294633 (89.2)  $[\text{C}_{42}\text{H}_{56}^{35}\text{Cl}^{63}\text{Cu}^{65}\text{CuN}_{10}]^+$ , 863.297988 (40.5)  $[\text{C}_{41}^{13}\text{CH}_{56}^{35}\text{Cl}^{63}\text{Cu}^{65}\text{CuN}_{10}]^+$ , 865.291683 (28.6)  $[\text{C}_{42}\text{H}_{56}^{37}\text{Cl}^{63}\text{Cu}^{65}\text{CuN}_{10}]^+$ , 866.295038 (13.0)  $[\text{C}_{41}^{13}\text{CH}_{56}^{37}\text{Cl}^{63}\text{Cu}^{65}\text{CuN}_{10}]^+$ , 867.289875 (6.4)  $[\text{C}_{42}\text{H}_{56}^{37}\text{Cl}^{65}\text{Cu}_2\text{N}_{10}]^+$ .

Powder diffraction confirms that the bulk essentially consists of the phase characterized by single crystal diffraction. NMR-spectroscopy was not possible since the crystals were not dissolvable in typical NMR solvents (Figure S1).

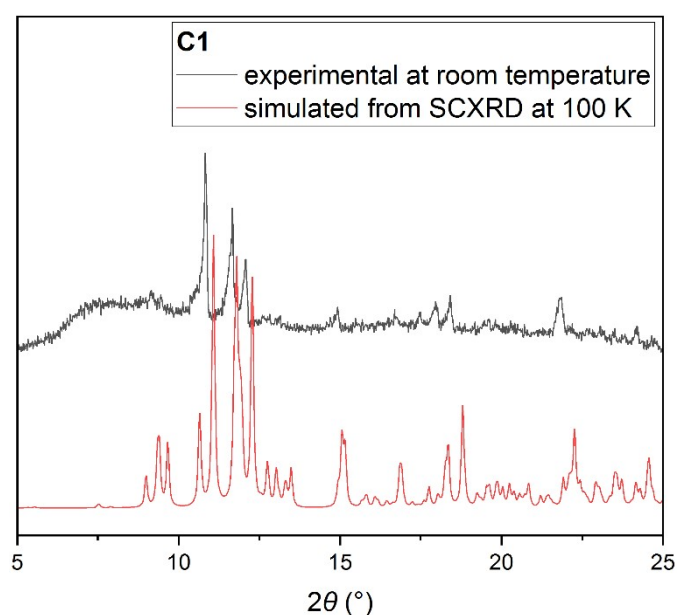


**Figure S1.** Simulated and experimental powder pattern of **C1**.

Additional information on the NMR spectra of the target compound including original data files is available via the Chemotion Repository: <https://dx.doi.org/10.14272/reaction/SA-FUHFF-UHFFFADPSC-UOUOYGYFRA-UHFFFADPSC-NUHFF-LUHFF-NUHFF-ZZZ>

### [Cu<sub>2</sub>{HC(3-<sup>t</sup>BuPz)<sub>2</sub>(CH<sub>2</sub>Py)}<sub>2</sub>Br<sub>2</sub>] C2

A solution of ligand **L1** (0.027 mmol, 1.0 eq., 18 mg) dissolved in MeOH (0.5 mL) was added dropwise to a solution of CuBr<sub>2</sub> (0.049 mmol, 1.8 eq., 11 mg) in MeOH (0.5 mL). The resulted yellow solution was filtered with a Whatman® filter. After 5 hours orange crystals suitable for XRD analysis were received.

IR (ATR,  $\tilde{\nu}$ ) = 2962 (w), 2861 (vw), 1592 (vw), 1560 (vw), 1460 (m), 1361 (w), 1346 (w), 1296 (vw), 1285 (vw), 1236 (m), 1167 (w), 1155 (w), 1059 (m), 1003 (w), 964 (w), 844 (m), 826 (w), 771 (vs), 728 (w), 663 (m), 556 (vw) cm<sup>-1</sup>.

MS (HR-ESI, MeOH):  $m/z$  (%) = (found) 905.2460 (50.3), 906.2489 (25.0), 907.2445 (100), 908.24708 (47.7), 909.2435 (65.2), 910.2455 (28.5), 911.24350 (16.5), 912.24455 (5.9) [M-Br]<sup>+</sup>; (calc.): 905.2459 (100) [C<sub>42</sub>H<sub>56</sub>N<sub>10</sub><sup>63</sup>Cu<sub>2</sub><sup>79</sup>Br]<sup>+</sup>, 906.2493 (45.4) [C<sub>42</sub><sup>13</sup>CH<sub>56</sub>N<sub>10</sub><sup>63</sup>Cu<sub>2</sub><sup>79</sup>Br]<sup>+</sup>, 907.2439 (97.3) [C<sub>42</sub>H<sub>56</sub>N<sub>10</sub><sup>63</sup>Cu<sub>2</sub><sup>81</sup>Br]<sup>+</sup>, 908.2472 (44.2) [C<sub>42</sub><sup>13</sup>CH<sub>56</sub>N<sub>10</sub><sup>63</sup>Cu<sub>2</sub><sup>81</sup>Br]<sup>+</sup>, 909.2421 (86.8) [C<sub>42</sub>H<sub>56</sub>N<sub>10</sub><sup>63</sup>Cu<sup>65</sup>Cu<sup>81</sup>Br]<sup>+</sup>, 910.2454(39.4) [C<sub>41</sub><sup>13</sup>CH<sub>56</sub>N<sub>10</sub><sup>63</sup>Cu<sup>65</sup>Cu<sup>81</sup>Br]<sup>+</sup>, 911.24036 (19.4) [C<sub>42</sub>H<sub>56</sub>N<sub>10</sub><sup>65</sup>Cu<sub>2</sub><sup>81</sup>Br]<sup>+</sup>, 912.2436 (8.8) [C<sub>41</sub><sup>13</sup>CH<sub>56</sub>N<sub>10</sub><sup>65</sup>Cu<sub>2</sub><sup>81</sup>Br]<sup>+</sup>.

Powder diffraction confirms that the bulk essentially consists of the phase characterized by single crystal diffraction. NMR-spectroscopy was not possible since the crystals were not dissolvable in typical NMR solvents (Figure S2).

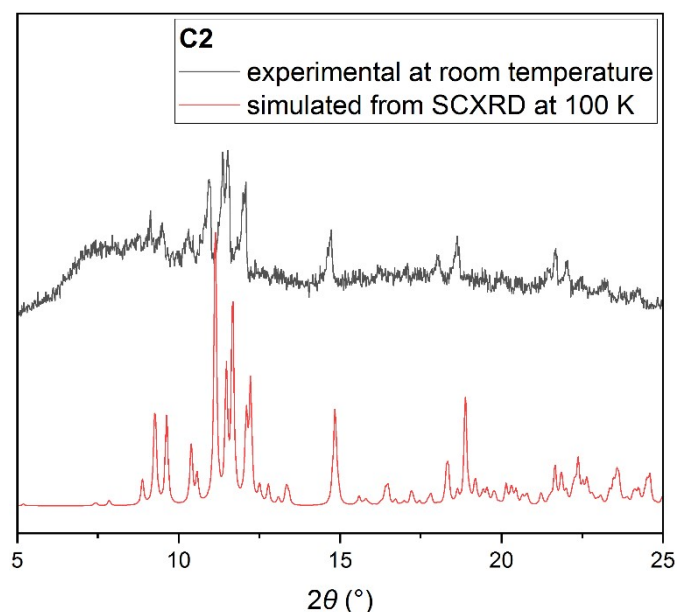


**Figure S2.** Simulated and experimental powder pattern of **C2**.

Additional information on the NMR spectra of the target compound including original data files is available via the Chemotion Repository: <https://dx.doi.org/10.14272/reaction/SA-FUHFF-UHFFFADPSC-GOAWIMPEEQ-UHFFFADPSC-NUHFF-LUHFF-NUHFF-ZZZ>

$[\text{Cu}_2\{\text{HC}(3\text{-}^t\text{BuPz})_2(\text{CH}_2\text{Py})\}_2\text{I}_2]$  **C3**

Ligand **L1** (0.0143 mmol, 1.00 eq., 10.0 mg) and CuI (0.032 mmol, 2.2 eq., 6.1 mg) were dissolved in DCM (1 mL). The pale-yellow colored solution showed yellow crystals after 1 day.

IR (ATR,  $\tilde{\nu}$ ) = 3111 (w), 2958 (w), 2927 (w), 2860 (w), 1600 (w), 1570 (w), 1522 (m), 1516 (m), 1482 (w), 1458 (s), 1434 (w), 1419 (w), 1364 (w), 1345 (w), 1330 (w), 1236 (s), 1207 (w), 1166 (w), 1156 (w), 1061 (m), 1012 (w), 1006 (w), 1002 (w), 963 (w), 844 (m), 825 (w), 815 (w), 800 (w), 781 (vs), 770 (vs), 747 (w), 728 (m), 667 (w), 662 (s), 640 (w), 605 (w), 582 (w), 554 (w), 496 (w), 490 (w), 451 (w), 441 (w), 438 (w), 427 (w), 397 (w), 374 (w), 359 (w), 354 (m), 348 (s), 344 (m), 339 (w), 332 (w), 324 (w), 317 (w), 314 (w), 311 (w), 307 (w), 304 (w), 302 (w), 297 (m), 288 (m), 285 (w), 282 (m), 278 (w), 274 (w), 271 (w), 266 (m), 261 (w), 255 (s)  $\text{cm}^{-1}$ .

MS (HR-ESI, MeOH):  $m/z$  (%) = (found) 953.23340 (100), 954.23602 (52.3), 955.23181 (99.0), 956.23307 (44.7), 957.23126 (28.8), 958.23236 (9.4), 959.23474 (1.7)  $[M-I]^+$ ; (calc.): 953.2320613 (100)  $[\text{C}_{42}\text{H}_{56}\text{N}_{10}^{63}\text{Cu}_2\text{I}]^+$ , 954.2354162 (45.4)  $[\text{C}_{41}^{13}\text{CH}_{56}\text{N}_{10}^{63}\text{Cu}_2\text{I}]^+$ , 955.2302533 (89.2)  $[\text{C}_{42}\text{H}_{56}\text{N}_{10}^{63}\text{Cu}^{65}\text{CuI}]^+$ , 956.2336082 (40.5)  $[\text{C}_{41}^{13}\text{CH}_{56}\text{N}_{10}^{63}\text{Cu}^{65}\text{CuI}]^+$ , 957.2284453 (19.9)  $[\text{C}_{42}\text{H}_{56}\text{N}_{10}^{65}\text{Cu}_2\text{I}]^+$ , 958.2318002 (9.0)  $[\text{C}_{41}^{13}\text{CH}_{56}\text{N}_{10}^{65}\text{Cu}_2\text{I}]^+$ , 959.2353 (4)  $[\text{C}_{40}^{13}\text{C}_2\text{H}_{56}\text{N}_{10}^{65}\text{Cu}_2\text{I}]^+$ .

Since only few crystals were received no further bulk analysis was possible.

Additional information on the NMR spectra of the target compound including original data files is available via the Chemotion Repository: <https://dx.doi.org/10.14272/reaction/SA-FUHFF-UHFFFADPSC-PVJIKXGCCG-UHFFFADPSC-NUHFF-LUHFF-NUHFF-ZZZ>

$[\text{Cu}_2\{\text{HC}(3\text{-}^t\text{BuPz})_2(\text{CH}_2\text{Py})\}_2](\text{PF}_6)_2$  **C4**

A solution of ligand **L1** (0.025 mmol, 1.0 eq., 18 mg) dissolved in DCM (2 mL) was added dropwise to  $[\text{Cu}(\text{MeCN})_4](\text{PF}_6)$  (18.6 mg, 0.05 mmol, 2.0 eq.). After filtration via Whatman® filter slow diffusion of pentane into the pale rose solution resulted colorless crystals after 1 week.

IR (ATR,  $\tilde{\nu}$ ) = 2970 (vw), 2871 (vw), 1603 (vw), 1575 (vw), 1522 (w), 1463 (w), 1364 (w), 1272 (w), 1172 (vw), 1067 (w), 1011 (vw), 968 (vw), 879 (w), 831 (vs), 733 (m), 705 (w), 664 (w)  $\text{cm}^{-1}$ .

MS (HR-ESI, MeOH):  $m/z$  (%) = (found) 413.1632 (100), 413.6650 (50.5), 414.1627 (98.9), 414.6640 (4.7) 415.1628 (28.7)  $[M]^{2+}$ ; (calc.) 413.16352 (100)  $[\text{C}_{42}\text{H}_{56}^{63}\text{Cu}_2\text{N}_{10}]^{2+}$ , 413.665197

(45.4)  $[\text{C}_{41}^{13}\text{CH}_5^6\text{Cu}^{63}\text{Cu}_2\text{N}_{10}]^{2+}$ , 414.162616 (89.5)  $[\text{C}_{42}\text{H}_5^6\text{Cu}^{65}\text{CuN}_{10}]^{2+}$ , 414.664293 (40.5)  $[\text{C}_{41}^{13}\text{CH}_5^6\text{Cu}^{65}\text{CuN}_{10}]^{2+}$ , 415.161712 (19.9)  $[\text{C}_{41}^{13}\text{CH}_5^6\text{Cu}^{65}\text{Cu}_2\text{N}_{10}]^{2+}$ .

Powder diffraction confirms that the bulk essentially consists of the phase characterized by single crystal diffraction. NMR-spectroscopy was not possible since the crystals were not dissolvable in typical NMR solvents (Figure S3).

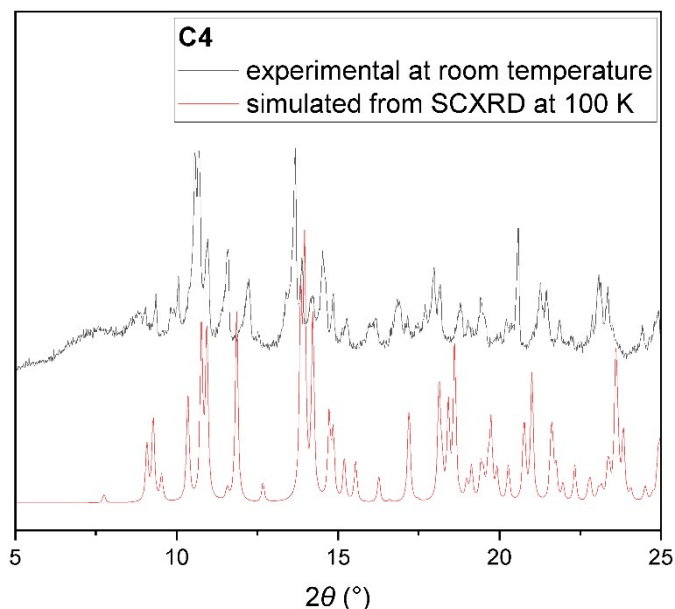


**Figure S3.** Simulated and experimental powder pattern of **C4**.

Additional information on the NMR spectra of the target compound including original data files is available via the Chemotion Repository: <https://dx.doi.org/10.14272/reaction/SA-FUHFF-UHFFFADPSC-LJKLVVBUTB-UHFFFADPSC-NUHFF-NUHFF-NUHFF-ZZZ>

$[\text{Cu}_2\{\text{HC}(3\text{-}^t\text{BuPz})_2(\text{CH}_2\text{Py})\}_2](\text{OTf})_2$  **C5**

**C5** was synthesized analogue to **C4** with  $[\text{Cu}(\text{MeCN})_4](\text{OTf})$ . Colorless crystals suitable for XRD analysis were received after 1 week.

IR (ATR,  $\tilde{\nu}$ ) = 3120 (vw), 2966 (w), 2933 (vw), 2906 (vw), 2869 (vw), 1603 (w), 1575 (vw), 1520 (w), 1485 (vw), 1466 (w), 1454 (w), 1435 (vw), 1421 (vw), 1361 (w), 1274 (s), 1255 (vs), 1235 (vs), 1226 (s), 1207 (w), 1164 (m), 1152 (m), 1060 (w), 1029 (vs), 1017 (w), 967 (w), 844 (w), 825 (w), 788 (m), 778 (s), 770 (m), 757 (w), 731 (w), 725 (w), 665 (m), 637 (vs), 607 (vw), 574 (w), 517 (m), 497 (vw)  $\text{cm}^{-1}$ .

MS (HR-ESI, MeOH):  $m/z$  (%) = (found) 413.1637 (100), 413.66533 (46.9), 414.1635 (94.6), 414.6644 (42.2), 415.1635 (26.8)  $[\text{M}]^{2+}$ ; (calc.): 413.16352 (100)  $[\text{C}_{42}\text{H}_5^6\text{Cu}^{63}\text{Cu}_2\text{N}_{10}]^{2+}$ , 413.665197 (45.4)  $[\text{C}_{41}^{13}\text{CH}_5^6\text{Cu}^{63}\text{Cu}_2\text{N}_{10}]^{2+}$ , 414.162616 (89.5)  $[\text{C}_{42}\text{H}_5^6\text{Cu}^{65}\text{CuN}_{10}]^{2+}$ , 414.664293 (40.5)  $[\text{C}_{41}^{13}\text{CH}_5^6\text{Cu}^{65}\text{CuN}_{10}]^{2+}$ , 415.161712 (19.9)  $[\text{C}_{41}^{13}\text{CH}_5^6\text{Cu}^{65}\text{Cu}_2\text{N}_{10}]^{2+}$ .

Powder diffraction confirms that the bulk essentially consists of the phase characterized by single crystal diffraction. NMR-spectroscopy was not possible since the crystals were not dissolvable in typical NMR solvents (Figure S4).

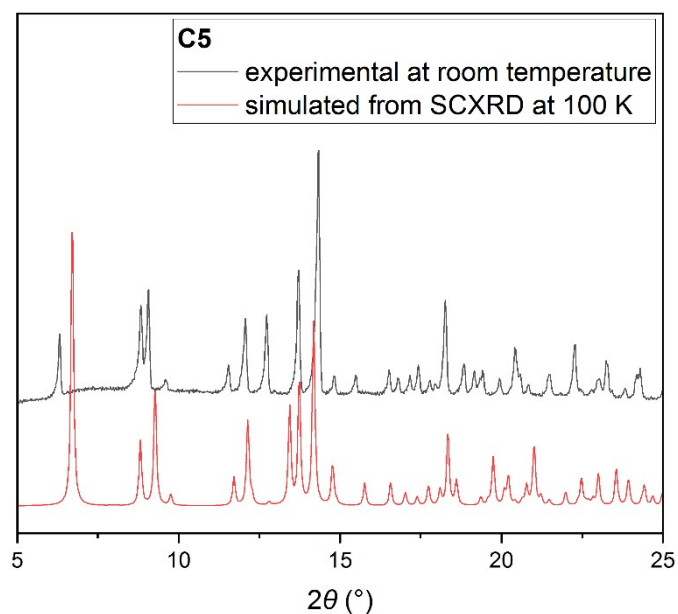


**Figure S4.** Simulated and experimental powder pattern of C5.

Additional information on the NMR spectra of the target compound including original data files is available via the Chemotion Repository: <https://dx.doi.org/10.14272/reaction/SA-FUHFF-UHFFFADPSC-HSMKDBCPZW-UHFFFADPSC-NUHFF-LUHFF-NUHFF-ZZZ>

## Preparation of the precursor solution $[\text{Cu}_2(\text{L1})]^{2+}(\text{SbF}_6^-)_2$ **C6**

Cu(I) chloride (0.129 mmol, 1.60 eq., 17.4 mg) and **L1** (0.080 mmol, 1.0 eq., 56 mg) were weighed into a degassed Schlenk tube covered with aluminum foil. After the addition of degassed DCM (5 mL), the solution was stirred overnight.  $\text{AgSbF}_6$  (0.183 mmol, 2.30 eq., 62.8 mg) was dissolved in degassed THF (0.25 mL) and under vigorous shaking, this solution was added dropwise to the Cu complex solution. After complete deposition of the  $\text{AgCl}$  precipitation, the precursor (15.2 mM) is obtained as a yellow colored solution.

## $[\text{Cu}_2(\text{HC}(3\text{-}^t\text{BuPz})_2(\text{CH}_2\text{Py}))_2\text{O}_2][\text{SbF}_6]_2$ **P**

Dry DCM (9.4 mL) was added to the UV/Vis spectroscopic measurement cell and saturated with oxygen by bubbling dioxygen through the solvent for 5 min. The precursor solution (0.650 mL, 15.2 mM) was added at rt resulting in the formation of the blue colored peroxido species (1.0 mM) within seconds.

Crystal: The precursor solution (see preparation of **C6**, 2 mL) in DCM was diluted with DCM (0.5 mL). After bubbling dioxygen through the solution (20 s) a deep blue color was observed. By slow diffusion of diethyl ether the complex **P** was received after one week at 3 °C as blue crystal blocks.

UV/Vis  $\lambda = 360$  nm ( $\epsilon \approx 18000$  L mol<sup>-1</sup> cm<sup>-1</sup>),  $\lambda = 560$  nm ( $\epsilon \approx 1000$  L mol<sup>-1</sup> cm<sup>-1</sup>).

HR-MS (ESI+, MeOH)  $m/z$  (%) =  $[\text{MSbF}_6]^+$ ; (found) 1093.2132 (3.6)  $[\text{C}_{42}\text{H}_{56}\text{N}_{10}^{63}\text{Cu}_2\text{O}_2^{121}\text{SbF}_6]^+$ , 1094.2134 (8.8)  $[\text{C}_{42}\text{H}_{56}\text{N}_{10}^{63}\text{Cu}_2\text{O}_2^{121}\text{SbF}_6]^+$ , 1095.2134 (15.3)  $[\text{C}_{42}\text{H}_{56}\text{N}_{10}^{63}\text{Cu}^{65}\text{CuO}_2^{121}\text{SbF}_6]^+$ , 1096.2136 (12.7)  $[\text{C}_{42}\text{H}_{56}\text{N}_{10}^{63}\text{Cu}^{65}\text{CuO}_2^{121}\text{SbF}_6]^+$ , 1097.2136 (8.0)  $[\text{C}_{42}\text{H}_{56}\text{N}_{10}^{63}\text{Cu}^{65}\text{CuO}_2^{123}\text{SbF}_6]^+$ , 1098.2146 (3.1)  $[\text{C}_{42}\text{H}_{56}\text{N}_{10}^{65}\text{Cu}_2\text{O}_2^{121}\text{SbF}_6]^+$ , 1099.2179 (1.9)  $[\text{C}_{42}\text{H}_{56}\text{N}_{10}^{65}\text{Cu}_2\text{O}_2^{123}\text{SbF}_6]^+$ ; (calc.): 1093.212 (100)  $[\text{C}_{42}\text{H}_{56}\text{N}_{10}^{63}\text{Cu}_2\text{O}_2^{121}\text{SbF}_6]^+$ , 1094.215 (45.4)  $[\text{C}_{42}\text{H}_{56}\text{N}_{10}^{63}\text{Cu}_2\text{O}_2^{121}\text{SbF}_6]^+$ , 1095.210 (89.2)  $[\text{C}_{42}\text{H}_{56}\text{N}_{10}^{63}\text{Cu}^{65}\text{CuO}_2^{121}\text{SbF}_6]^+$ , 1096.21 (40.5)  $[\text{C}_{42}\text{H}_{56}\text{N}_{10}^{63}\text{Cu}^{65}\text{CuO}_2^{121}\text{SbF}_6]^+$ , 1097.21 (66.73)  $[\text{C}_{42}\text{H}_{56}\text{N}_{10}^{63}\text{Cu}^{65}\text{CuO}_2^{123}\text{SbF}_6]^+$ , 1098.214 (30.3)  $[\text{C}_{42}\text{H}_{56}\text{N}_{10}^{65}\text{Cu}_2\text{O}_2^{121}\text{SbF}_6]^+$ , 1099.208 (14.9)  $[\text{C}_{42}\text{H}_{56}\text{N}_{10}^{65}\text{Cu}_2\text{O}_2^{123}\text{SbF}_6]^+$ .

HR-MS (ESI+, MeOH)  $m/z$  (%) =  $[\text{M}]^{2+}$ ; found: 429.1589 (3.6)  $[\text{C}_{42}\text{H}_{56}\text{N}_{10}^{63}\text{Cu}_2\text{O}_2]^{2+}$ , 429.6605 (1.8)  $[\text{C}_{42}\text{H}_{56}\text{N}_{10}^{63}\text{Cu}_2\text{O}_2]^{2+}$ , 430.1585 (1.6)  $[\text{C}_{42}\text{H}_{56}\text{N}_{10}^{63}\text{Cu}^{65}\text{CuO}_2]^{2+}$ , 430.6597 (1.2)  $[\text{C}_{42}\text{H}_{56}\text{N}_{10}^{63}\text{Cu}^{65}\text{CuO}_2]^{2+}$ , 431.1598 (1.2)  $[\text{C}_{42}\text{H}_{56}\text{N}_{10}^{65}\text{Cu}_2\text{O}_2]^{2+}$ , 431.66098 (0.5)  $[\text{C}_{42}\text{H}_{56}\text{N}_{10}^{65}\text{Cu}_2\text{O}_2]^{2+}$ ; (calc.): 429.1584 (100)  $[\text{C}_{42}\text{H}_{56}\text{N}_{10}^{63}\text{Cu}_2\text{O}_2]^{2+}$ , 429.6601 (45.4)  $[\text{C}_{42}\text{H}_{56}\text{N}_{10}^{63}\text{Cu}_2\text{O}_2]^{2+}$ , 430.1575 (89.2)  $[\text{C}_{42}\text{H}_{56}\text{N}_{10}^{63}\text{Cu}^{65}\text{CuO}_2]^{2+}$ , 430.6592 (40.5)  $[\text{C}_{42}\text{H}_{56}\text{N}_{10}^{63}\text{Cu}^{65}\text{CuO}_2]^{2+}$ , 431.1566 (19.9)  $[\text{C}_{42}\text{H}_{56}\text{N}_{10}^{65}\text{Cu}_2\text{O}_2]^{2+}$ , 431.6583 (9.04)  $[\text{C}_{42}\text{H}_{56}\text{N}_{10}^{65}\text{Cu}_2\text{O}_2]^{2+}$ .

Additional information on the NMR spectra of the target compound including original data files is available via the Chemotion Repository: <https://dx.doi.org/10.14272/reaction/SA-FUHFF-UHFFFADPSC-AIPOEOWGXQ-UHFFFADPSC-NUHFF-NUHFF-NUHFF-ZZZ>

## UV/Vis spectroscopic Experiments

### Temperature dependence of the peroxido formation

The peroxido species **P** was synthesized according to the method described above. In this case, DCM (9.4 mL) is saturated with dioxygen at different temperatures (-78 °C, -60 °C and rt). The solution was held constant at this temperature while adding the precursor solution (650 µL) and the peroxido formation was followed via UV/Vis spectroscopy.

In order to determine a suitable solvent for the formation of **P** the solvent added to the UV/Vis measurement cell was varied. Accordingly, DCM, THF and acetone were used as solvent.

### Stability of the peroxido towards different bases

After complete formation of the peroxido complex (0.01 mmol, 1 eq.) in DCM at rt, the base (1.00 mmol, 100 eq.) was added and the reaction was followed via UV/Vis spectroscopy. Stability tests were performed using the bases NEt<sub>3</sub>, DBU, DANCO, diethylamine, diisopropylamine and pyridine.

### Substrate hydroxylation catalysis

To the peroxido complex (1 mM) in DCM (10 mL) at rt a solution of the substrate (25 or 50 eq.) and NEt<sub>3</sub> (50 or 100 eq.) in DCM or THF was added and the reaction was monitored via UV/Vis spectroscopy.

For subsequent coupling reaction, *o*-phenylenediamine (25 or 50 eq.) was dissolved in DCM or THF and added to the solution after terminated hydroxylation reaction. The resulting reaction mixture was stirred at rt overnight and it was terminated by addition of EDTA and HCl (0.5 M, 2-4 mL). After extraction with DCM (3 x 20 mL) the combined organic layers were dried over MgSO<sub>4</sub> and solvent was removed under reduced pressure. For scale-up of the catalytic reactions, the resulting product mixture was purified via column chromatography.

### Ligand recycling

After scaling-up the catalysis, the product mixture was purified via column. Solvent system varied dependent on the product investigated. As the first fraction the ligand was obtained. For different catalysis experiments these ligand fractions were collected and purified again via column chromatography (acetone: hexane 1:4). The obtained ligand crystallized as a white solid. Subsequent precursor synthesis and catalysis experiments were performed according to previously described methods.

## Characterization of L1

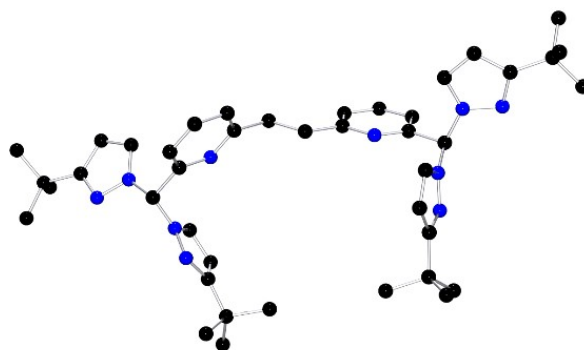


**Figure S5.** Molecular structure in the solid state of **L1**. Hydrogen atoms were omitted for clarity.

After successful synthesis, ligand **L1** was crystallized from ethyl acetate and its molecular structure was determined via single crystal X-ray crystallography (Figure S5). The ligand crystallizes in the monoclinic space group *Cc*. Comparing the molecular structure of the ligand **L1** to well-known and characterized bis(pyrazolyl)methane ligands, bond angles as well as bond length show high similarities. Additionally, a characteristic structural element is the slightly distorted tetrahedral geometry of the central C atom  $C_{ap}$ .<sup>38,39</sup>

## Molecular structures of C1-C5 in the solid state

The complexes **C1** [Cu<sub>2</sub>(L1)Cl<sub>2</sub>], **C2** [Cu<sub>2</sub>(L1)Br<sub>2</sub>] and **C3** [Cu<sub>2</sub>(L1)I<sub>2</sub>] exhibit four crystallographically independent molecules per crystallographic cell. Table S2 displays a detailed overview over selected bond length and angles.

**Table S2.** Selected bond lengths and angles of **C1** [Cu<sub>2</sub>(L1)Cl<sub>2</sub>], **C2** [Cu<sub>2</sub>(L1)Br<sub>2</sub>], **C3** [Cu<sub>2</sub>(L1)I<sub>2</sub>], **C4** [Cu<sub>2</sub>(L1)(MeCN)<sub>2</sub>](PF<sub>6</sub>)<sub>2</sub> and **C5** [Cu<sub>2</sub>(L1)(MeCN)<sub>2</sub>](OTf)<sub>2</sub>.

	<b>C1</b>	<b>C2</b>	<b>C3</b>	<b>C4</b>	<b>C5</b>
X =	Cl	Br	I	MeCN	MeCN
<b>Bond length [Å]</b>					
Cu-N <sub>Pz,1</sub>	2.140(2)	2.140(5)	2.097(8)		
	2.088(2)	2.079(5)	2.118(7)		
	2.141(2)	2.118(5)	2.125(7)	2.091(3)	2.073(2)
	2.102(2)	2.098(5)	2.111(7)		
Cu-N <sub>Pz,2</sub>	2.1310(19)	2.159(5)	2.161(8)		
	2.140(2)	2.150(5)	2.186(9)		
	2.148(2)	2.129(5)	2.170(8)	2.117(3)	2.123(2)
	2.109(2)	2.117(5)	2.146(7)		
Cu-N <sub>Py</sub>	2.1087(19)	2.117(5)	2.164(7)		
	2.1115(19)	2.118(5)	2.156(8)		
	2.1174(19)	2.104(5)	2.141(6)	2.116(3)	2.083(2)
	2.1128(19)	2.114(5)	2.161(8)		
Cu-X	2.2165(8)	2.3397(11)	2.504(2)		
	2.2000(8)	2.3261(11)	2.504(2)		
	2.2165(8)	2.3367(11)	2.500(2)	1.905(3)	1.887(2)
	2.2051(8)	2.3304(11)	2.503(2)		
<b>Bond angles [°]</b>					
N <sub>Pz,1</sub> -Cu-X	126.49(6)	128.26(14)	128.88(18)		
	127.34(6)	128.78(15)	129.55(19)		
	127.05(6)	128.98(14)	131.2(2)	124.31(13)	127.34(10)
	125.67(6)	125.87(14)	126.2(2)		
N <sub>Pz,2</sub> -Cu-X	121.94(6)	121.16(15)	119.94(19)		
	120.58(6)	119.39(14)	120.3(3)		
	122.00(6)	120.45(15)	118.82(18)	127.57(13)	119.42(10)
	122.92(6)	122.50(14)	122.66(19)		
N <sub>Pz,1</sub> -Cu-N <sub>Pz,2</sub>	90.53(7)	89.3(2)	89.4(3)		
	88.10(7)	88.49(19)	88.7(3)		
	89.68(8)	90.5(2)	90.7(3)	90.34(12)	91.70(9)
	88.30(8)	88.8(2)	89.2(3)		
N <sub>Pz,1</sub> -Cu-N <sub>Py</sub>	87.31(7)	89.74(19)	90.3(3)		
	90.00(7)	89.9(2)	90.6(3)		
	88.92(8)	87.3(2)	87.0(2)	88.80(12)	90.42(9)
	89.65(7)	89.66(19)	90.0(3)		
N <sub>Pz,2</sub> -Cu-N <sub>Py</sub>	90.28(7)	91.30(19)	92.7(3)		
	91.30(7)	92.57(19)	92.9(3)		
	90.04(7)	91.78(19)	93.7(3)	89.44(12)	87.52(9)
	91.75(8)	92.27(19)	91.8(3)		
$\tau_4 = \frac{360^\circ - (\alpha + \beta)}{141}$	0.79	0.78	0.75	0.77	0.80

## Characterization of **P** with Density Functional Theory

In order to obtain more detailed information about structure and coordination geometry of the peroxido species, **P** was characterized via XRD. Blue crystals were obtained by slow diffusion of diethyl ether into a solution of **P** at 3 °C. The resulting structure is displayed in Figure S40.

Experimental Data, obtained via XRD and UV/Vis was in the following compared to theoretical calculations. Therefore, DFT calculations were performed with TPSSh def2-TZVP and GD3BJ for **P** the gas phase. After calculating the optimized structure (Table S3), UV/Vis spectrum and corresponding NTOs were calculated (Figure S6).

**Table S3.** Selected bond lengths and Cu...Cu vector of the peroxido complex cation **P**<sup>2+</sup>. DFT calculations were performed with TPSSh def2-TZVP and GD3BJ in the gas phase.

	Bond lengths and Cu..Cu vector [Å]	
	Calculated	Crystal structure
Cu-Cu	3.606	3.551
Cu-O(1)	1.976	1.930(2) 1.918(2)
Cu-O(2)	1.916	1.9365(19) 1.939(2)
Cu-N(Pz,1)	2.028	1.993(2) 1.999(2)
Cu-N(Pz,2)	1.987	2.124(2) 2.035(2)
Cu-N(py)	2.340	2.200(2) 2.302(2)
O-O	1.428	1.480(3)

**Table S4.** Geometric key parameters with TPSSh def2-TZVP and GD3BJ in the gas phase

	S2	Energy in H	relative E in kcal/mol
Singlet Oxo		-5613,96008300	17.7
Singlet Peroxo		-5613,98439930	15.3
Peroxo BS	0.48	-5613,98823730	0.00

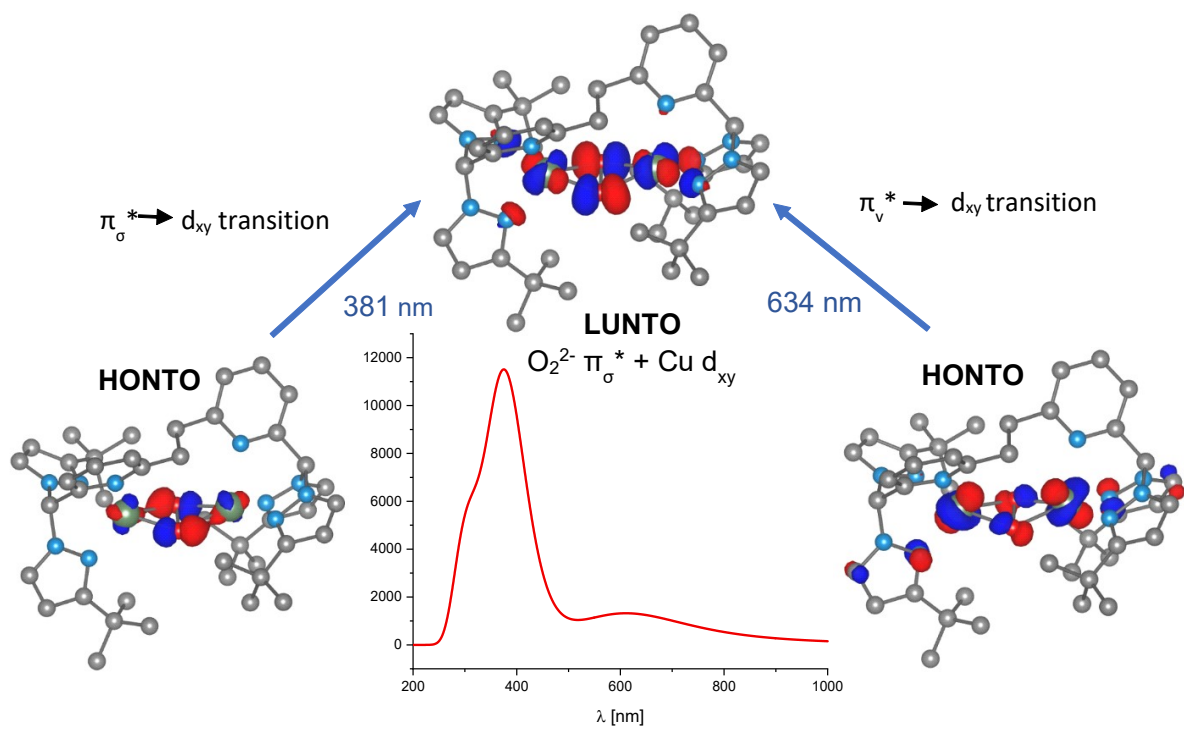


**Figure S6.** UV/Vis spectrum of the [Cu<sub>2</sub>O<sub>2</sub>{HC(3-tBuPz)<sub>2</sub>(CH<sub>2</sub>Py)}<sub>2</sub>][SbF<sub>6</sub>]<sub>2</sub> (**P**) calculated via TD-DFT and NTO-analysis of **P** for the transitions of 381 nm and 634 nm in the gas phase.

## UV/Vis spectroscopic Experiments characterizing properties of P

### Temperature dependency of the formation and stability of P

According to the general procedure of the preparation of the precursor solution and the subsequent UV/Vis spectroscopic monitoring of the formation of P, the influence of solvent and temperature on the oxygen activation was investigated.

First, the temperature was varied between  $-80\text{ }^{\circ}\text{C}$ ,  $-60\text{ }^{\circ}\text{C}$  and room temperature using dioxygen saturated, dry DCM as solvent and a precursor concentration of 1 mM. In the following, UV/Vis spectra of different times after addition of the precursor solution into the dioxygen saturated DCM are displayed at  $-80\text{ }^{\circ}\text{C}$  (Figure S7),  $-60\text{ }^{\circ}\text{C}$  (Figure S8) and at room temperature (Figure S9) are displayed. Furthermore, the absorbance at the absorption maximum at 359 nm at different times after precursor injection is plotted against the time.

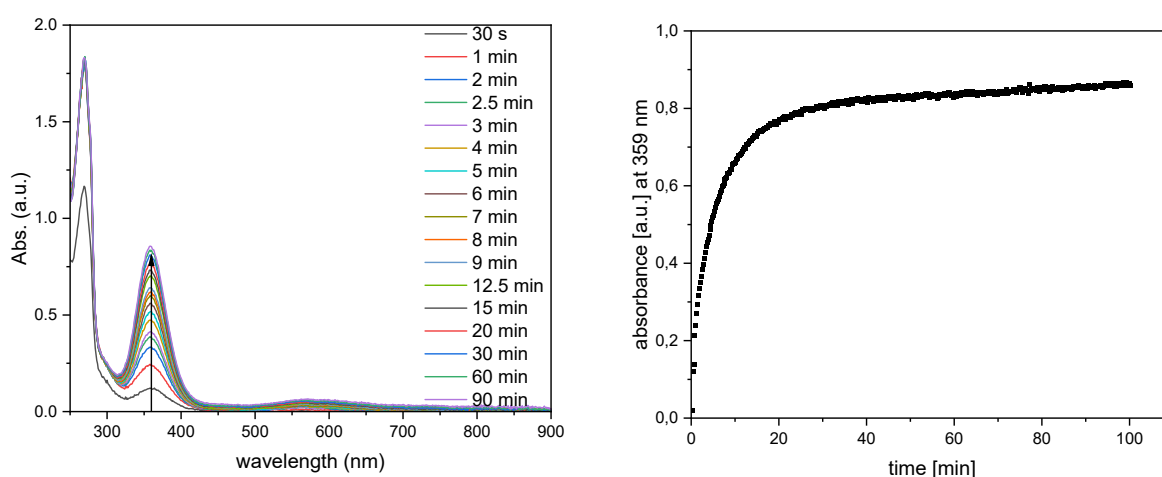


**Figure S7.** Formation of P in dioxygen saturated DCM at different times after precursor (1 mM) addition at  $-80\text{ }^{\circ}\text{C}$ . Left: UV/Vis spectra at different times, right: Absorbance at 359 nm plotted versus the time.

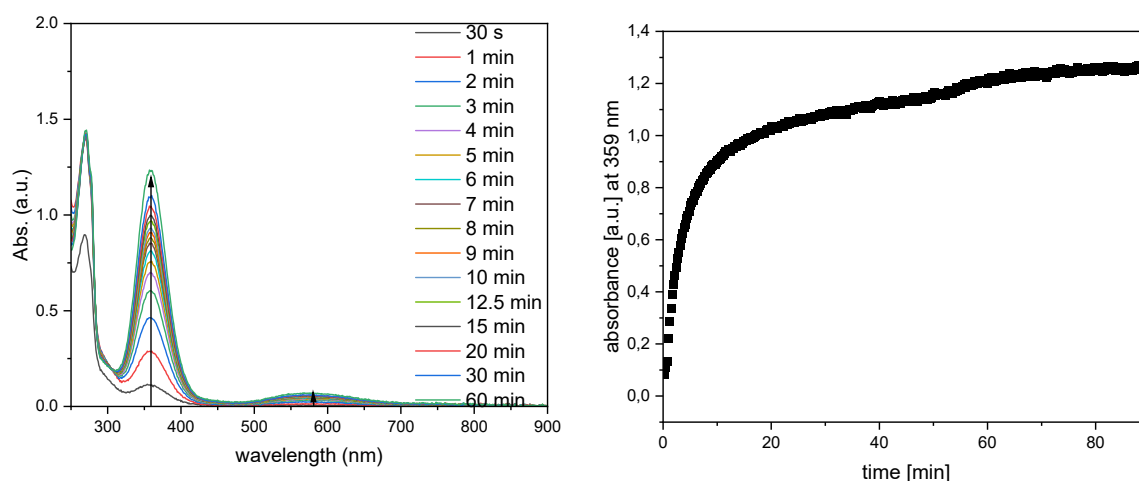


**Figure S8.** Formation of P in dioxygen saturated DCM at different times after the precursor (1 mM) addition at  $-60\text{ }^{\circ}\text{C}$ . Left: UV/Vis spectra at different times, right: Absorbance at 359 nm plotted versus the time.

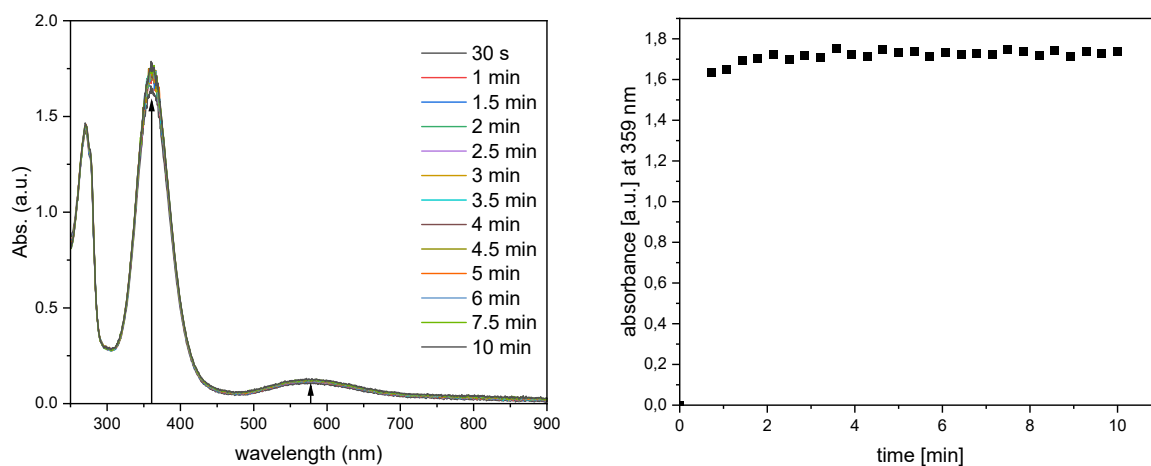


**Figure S9.** Formation of **P** in dioxygen saturated DCM at different times after the precursor (1 mM) addition at room temperature. Left: UV/Vis spectra at different times, right: Absorbance at 359 nm plotted versus the time.

Investigating the stability of **P** at room temperature, a freshly prepared solution of the **P** (1mM) in DCM was stirred at room temperature and monitored via UV/Vis spectroscopy for 17 h. The absorbance of the absorbance maximum at 359 nm is plotted vs the time (Figure S10).

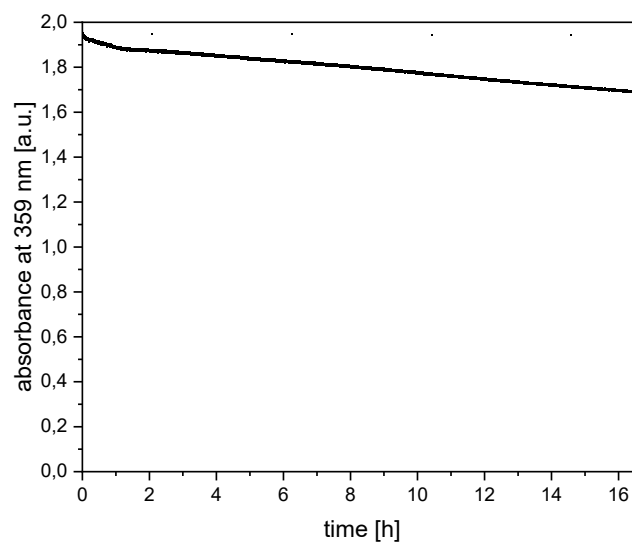


**Figure S10.** UV/Vis absorbance at  $\lambda = 359$  nm dependent on the time at room temperature in DCM  $c(\mathbf{P}) = 1$  mM.

## Solvent Influence on the formation of P

In order to investigate the suitability of different solvent systems, the formation of the peroxido species at room temperature was investigated in DCM, THF (Figure S11) and acetone (Figure S12) via UV/Vis spectroscopy. For all three solvents the formation of the peroxido complex P was observed. However, the formation in THF and acetone and is not complete and the smallest ratio of peroxido formation is observed in acetone. Furthermore, stability of P in DCM is higher than in THF (Figure S10 and Figure S11).

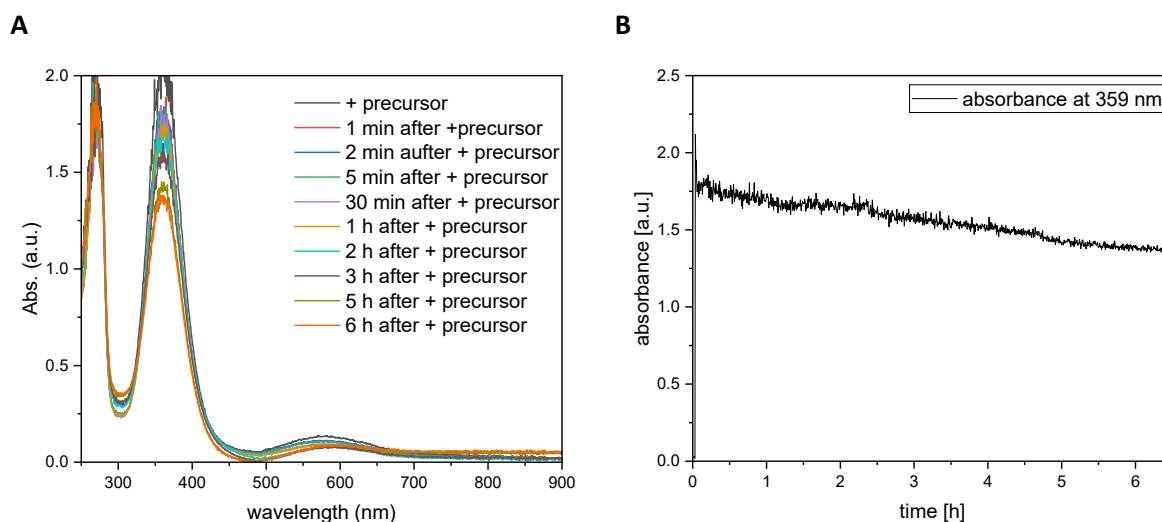


**Figure S11.** UV/Vis spectra of the formation of P in dioxxygen saturated THF at different times after the precursor (1 mM) addition at rt (A) and absorbance at 359 nm during 6.5 h at rt (B).

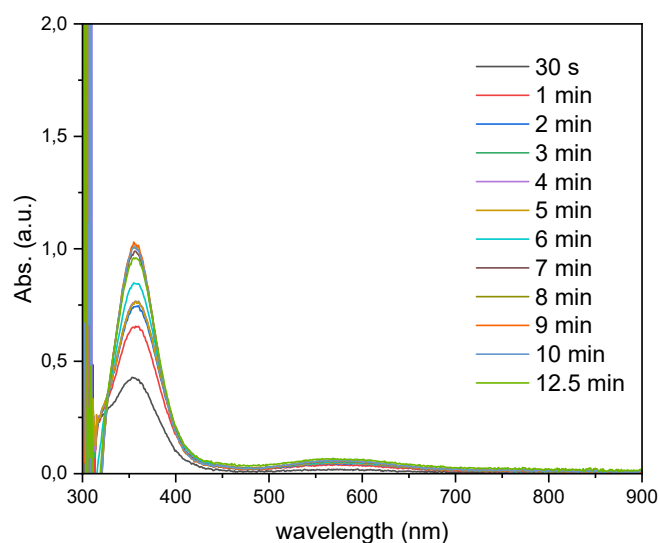


**Figure S12.** UV/Vis spectra of the formation of P in dioxxygen saturated acetone at different times after the precursor (1 mM) addition at rt.

## Stability of **P** towards water and bases

In order to find a suitable auxiliary base for the substrate conversion, the stability of **P** towards different bases was investigated.

After formation of peroxido complex **P** in dry DCM at room temperature, the base was added and the resulting reaction was monitored via UV/Vis-spectroscopy. The bases a) 1,4-Diazabicyclo[2.2.2]octane (DABCO) , b) 1,8-Diazabicyclo[5.4.0]undec-7-en (DBU), c) diethylamine (HNEt<sub>2</sub>), d) diisopropylamine , e) pyridine and f) triethylamine (NEt<sub>3</sub>) were analyzed regarding their suitability as auxiliary base for the substrate conversion with **P**. Resulting UV/Vis spectra are depicted in Figure S13.

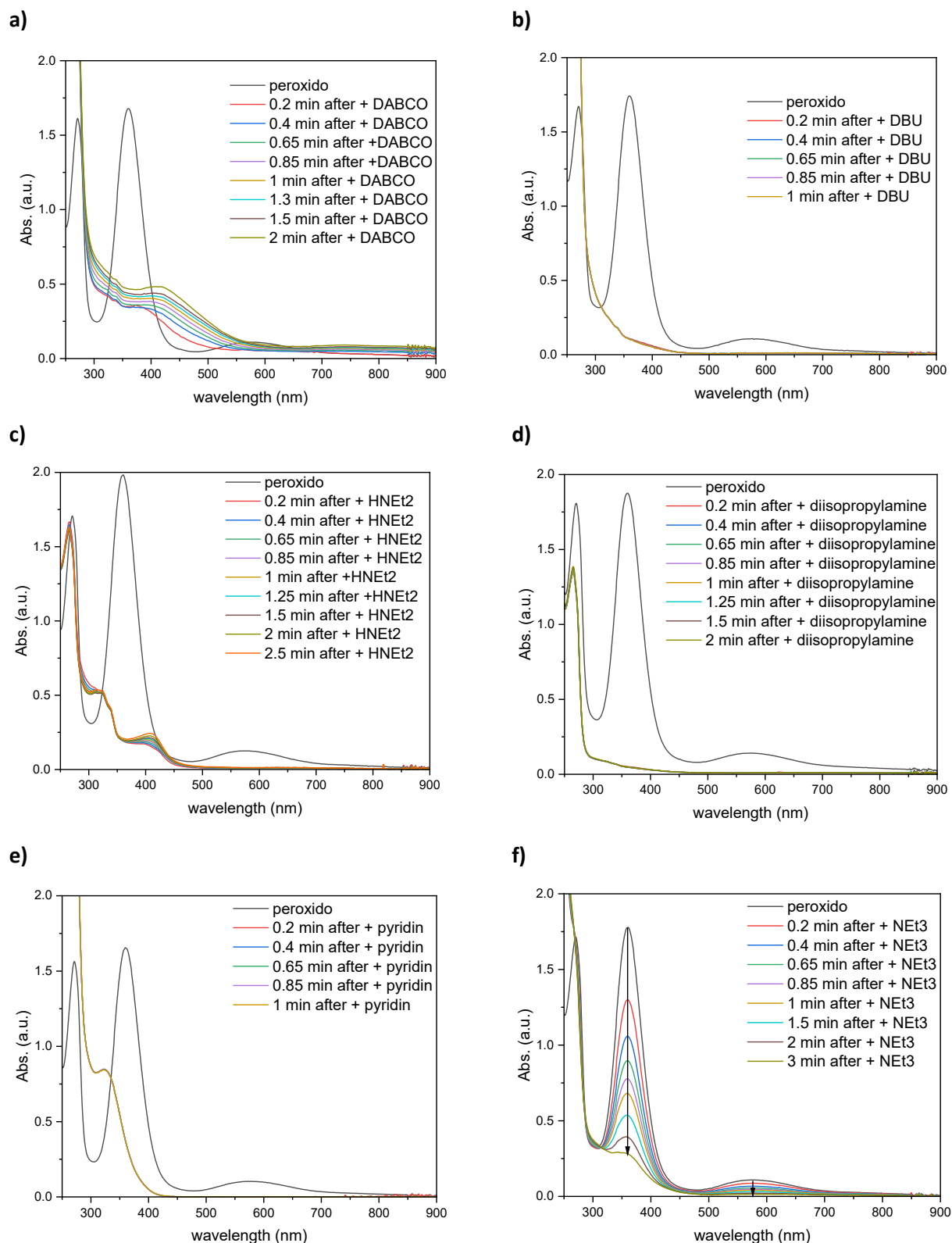


**Figure S13.** UV/Vis spectra of the formation of P in DCM (1 mM) at room temperature and the subsequent addition of base solution (100 eq.) a) 1,4-Diazabicyclo[2.2.2]octane (DABCO), b) 1,8-Diazabicyclo[5.4.0]undec-7-en (DBU), c) diethylamine (HNEt<sub>2</sub>), d) diisopropylamine, e) pyridine, f) triethylamine (NEt<sub>3</sub>).

According to the recorded spectra, triethylamine was used as auxiliary base for all following substrate conversions.

## Substrate Catalysis

Catalytic properties of **P** were investigated performing UV/Vis spectroscopy experiments and scale-up experiments as described in the experimental section. Below, the UV/Vs spectra of the addition of a substrate solution containing the substrate (25 eq. or 50 eq.) and triethylamine (50 eq. or 100 eq.) to a solution of **P** in DCM are displayed. Next to the conversion of 2-naphthol (Figure S14), measurements with 1-naphthol (Figure S15) and 4-hydroxycarbazole (Figure 16) are monitored via UV/Vis-spectroscopy.

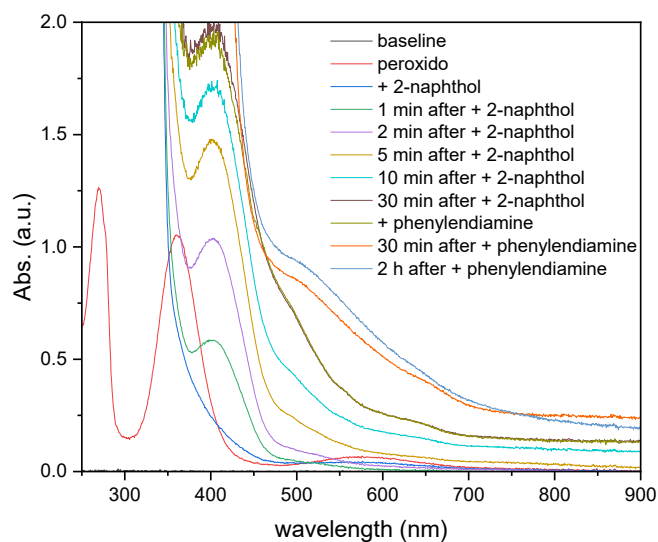


**Figure S14.** UV/Vis spectrum of the formation of **P** in DCM (1 mm) at room temperature, the subsequent addition of substrate solution (2-naphthol (50 eq.) and  $\text{NEt}_3$  (100 eq.)) and the addition of phenylendiamine (50 eq.).

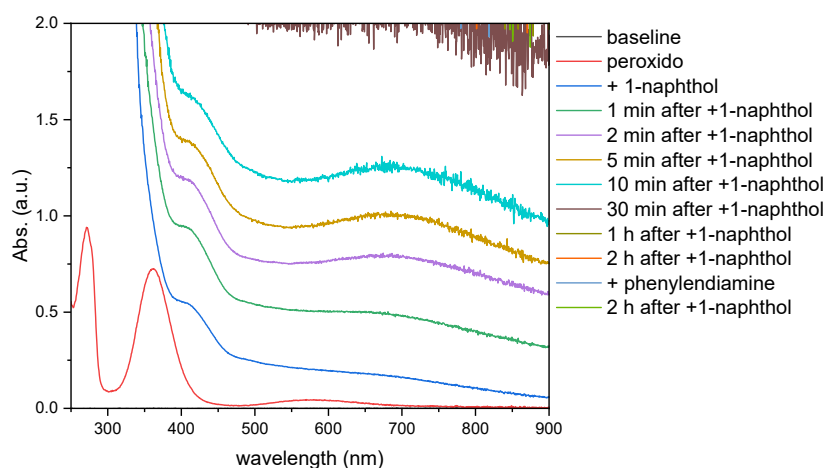


**Figure S15.** UV/Vis spectrum of the formation of **P** in DCM (1 mm) at room temperature, the subsequent addition of substrate solution (1-naphthol (50 eq.) and  $\text{NEt}_3$  (100 eq.)) and the addition of phenylendiamine (50 eq.).

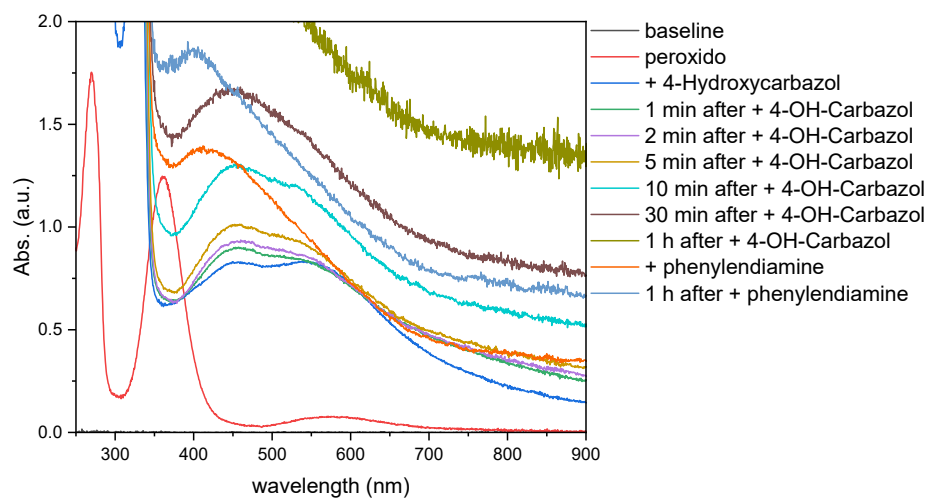


**Figure 16.** UV/Vis spectrum of the formation of **P** in DCM (1 mm) at room temperature, the subsequent addition of substrate solution (4-Hydroxycarbazol (50 eq.) and  $\text{NEt}_3$  (100 eq.)) and the addition of phenylendiamine (50 eq.).

## Ligand Recycling

During product isolation of scale-up catalysis experiments via column chromatography, the ligand **L1** could be isolated as well with up to 58 % yield. The collected recycled ligand fractions from various catalysis tests were again purified via column chromatography (hexane : ethyl acetate = 4:1, rf = 0.38). The ligand was obtained as a white solid which could be crystallized in ethyl acetate.

Purity of **L1** was proven by  $^1\text{H-NMR}$  (Figure S17).

$^1\text{H-NMR}$  (400 MHz,  $\text{CDCl}_3$ ):  $\delta$  = 7.55 (s, 2 H; CH), 7.45 (t,  $3J_{\text{H,H}} = 7.8$  Hz, 2 H; 3-H(py)), 7.28 (d,  $^3J_{\text{H,H}} = 2.2$  Hz, 4 H; 1-H(pz)), 6.90 (d,  $^3J_{\text{H,H}} = 8.1$  Hz, 2H; 4-H(py)), 6.69 (d,  $^3J_{\text{H,H}} = 7.8$  Hz, 2 H; 2-H(py)), 6.11 (d,  $^3J_{\text{H,H}} = 2.4$  Hz, 4 H; 2-H(pz)), 3.15 (s, 4 H;  $\text{CH}_2$ ), 1.28 (s, 36 H; H(tBu)) ppm.

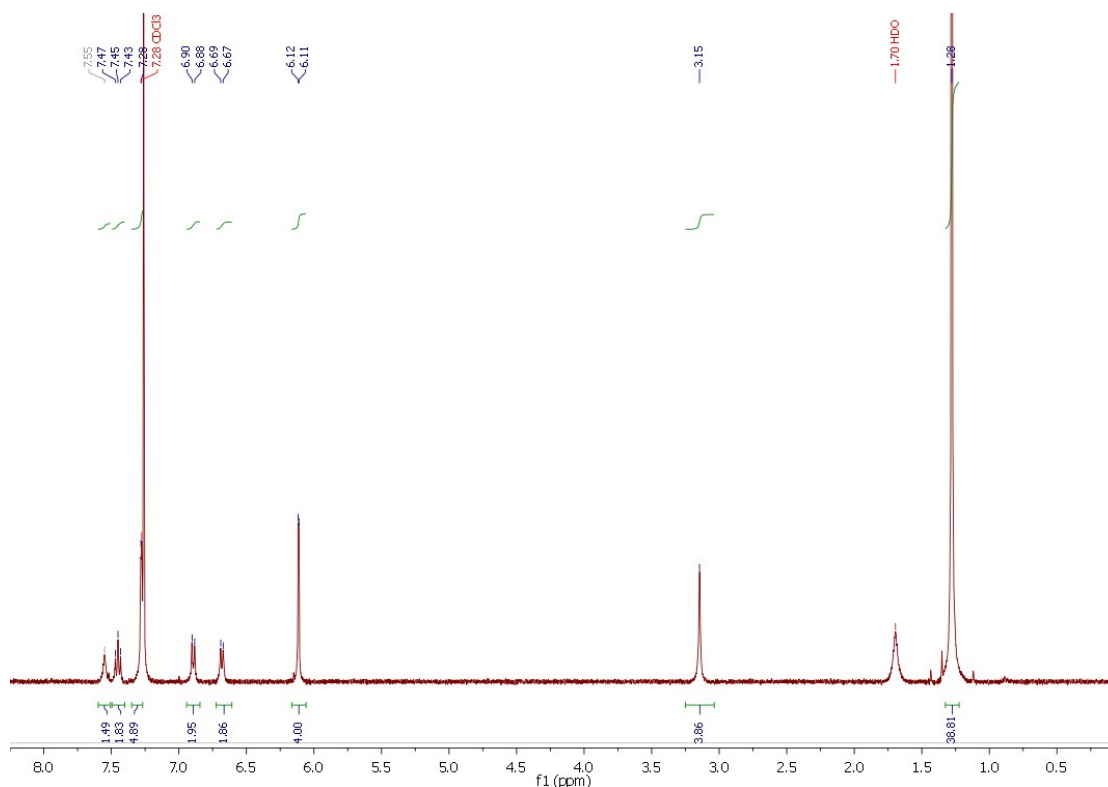
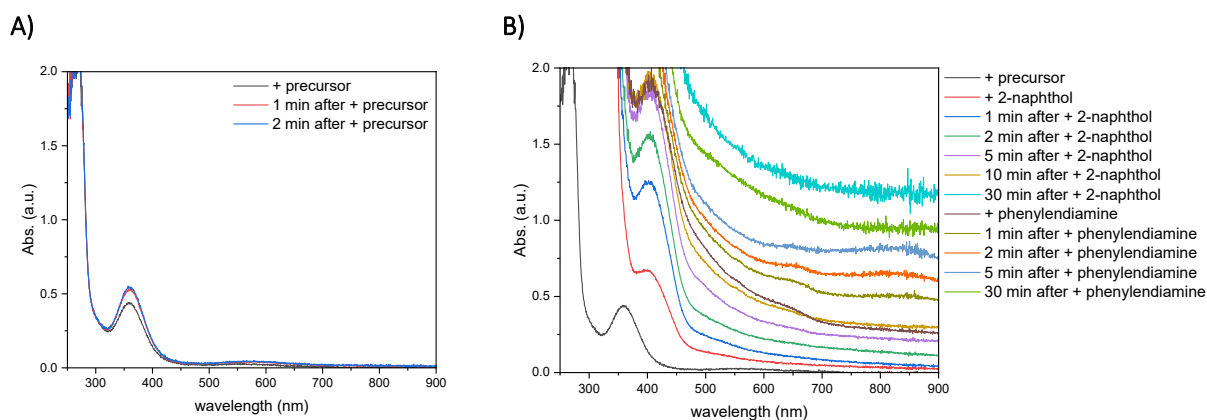


Figure S17.  $^1\text{H-NMR}$  spectrum of **L1** after ligand recycling.

Furthermore, oxygenation and catalysis experiments were performed using the recycled ligand **L1**. Formation of **P** could be observed, however with a smaller yield than shown in previous experiments (Figure S18). This difference can be explained by the sensitive precursor preparation. The amount of recycled ligand was small, therefore a small precursor batch was prepared. Some steps of the precursor synthesis like the precipitation of AgCl and the subsequent separation of the precursor solution are less efficient with small volumes thus the formation of **P** is less for this experiment. Conversion of the substrate 2-naphthol (50 eq.) with triethylamine (100 eq.) shows, that also the recycled ligand **L1** forms a catalytically active peroxido complex **P** and thus indicates a successful ligand recycling (Figure S18).



**Figure S18.** UV/Vis -spectra of the formation of **P** in DCM at rt ( $c(\text{precursor})=1\text{mm}$ ) A) and subsequent addition of 2-naphthol (50 eq.), Triethylamine (100 eq.) and phenylendiamine (50 eq.) after ligand recycling B).

## CV measurements

Preparation of the solutions:

Precursor solution  $[\text{Cu}_2(\text{L1})](\text{SbF}_6)$  (**C6**) was prepared like described above and diluted afterwards by adding the prepared solution (0.15 mL, 4.5 mmol) to degassed DCM (4.85 mL). Tetrabutylammonium hexafluorophosphate (194 mg, 0.500 mmol) was added.

Complex solutions of **C4**  $[\text{Cu}_2(\text{L1})(\text{MeCN})_2](\text{PF}_6)_2$  and **C5**  $[\text{Cu}_2(\text{L1})(\text{MeCN})_2](\text{OTf})_2$  were prepared in situ.  $[\text{Cu}(\text{MeCN})_4](\text{PF}_6)$  (6.1 mg, 0.016 mmol, 2.0 eq.) respectively  $[\text{Cu}(\text{MeCN})_4](\text{OTf})$  (6.1 mg, 0.016 mmol, 2.0 eq.) was dissolved in MeCN (1 mL) and added to **L1** (5.7 mg, 0.0081 mmol, 1.0 eq.). The complex solution was added to a solution of tetrabutylammonium hexafluorophosphate (194 mg, 0.500 mmol) in MeCN (4 mL).

Cyclic voltammetric measurements of the precursor complex were not reproducible and exhibited a decomposition reaction during the measurement (see Figure S19). Since **C6** is prepared by precipitation of the coordinating choro ligand with silver hexafluoroantimonate, it is possible that dissolved silver ions remain in the solution and distort the CV measurements. Additionally, **C6** exhibits a high reactivity due to its free coordination sites which makes it susceptible for decay reactions.

So, for the CV measurements the copper(I) complexes **C4** and **C5** in acetonitrile were investigated (see Figure S20 - Figure S23). Since **L1** exhibits two coordination sites, it is possible that only one copper centre is coordinated which can feature an additional peak in the cyclo voltammogram. So, an additional measurement with a similar mononucleating ligand (HC(3-*t*BuPz)<sub>2</sub>Py) (2-(bis(3-(*tert*-butyl)-1*H*-pyrazol-1-yl)methyl)pyridine <sup>40</sup> **L3**) with  $[\text{Cu}(\text{MeCN})_4]\text{PF}_6$  to form **C7** was performed (see Figure S24 and Figure S25).

Complex solution of **C7**  $[\text{Cu}(\text{L3})(\text{MeCN})]\text{PF}_6$  was prepared in situ.  $[\text{Cu}(\text{MeCN})_4](\text{PF}_6)$  (6.1 mg, 0.0163 mmol, 1.0 eq.) was dissolved in MeCN (1 mL) and added to **L3** (5.5 mg, 0.016 mmol, 1.0 eq.). The complex solution was added to a solution of tetrabutylammonium hexafluorophosphate (194 mg, 0.500 mmol) in MeCN (4 mL).

For the CV measurements of **P** the precursor complex (0.20 mL, 6.0 mmol) was added to DCM (5 mL, saturated with oxygen for 5 min at -80 °C and then warmed up to rt) under stirring. After 10 min, **P** was formed completely and the solution was degassed via freeze-pump-thaw (3 cycles). Tetrabutylammonium hexafluorophosphate (194 mg, 0.500 mmol) was added.

All spectra exhibit non-reversible behavior, qualitatively the cyclic voltammograms of **C4** and **C5** display the same CV waves like **C7**.

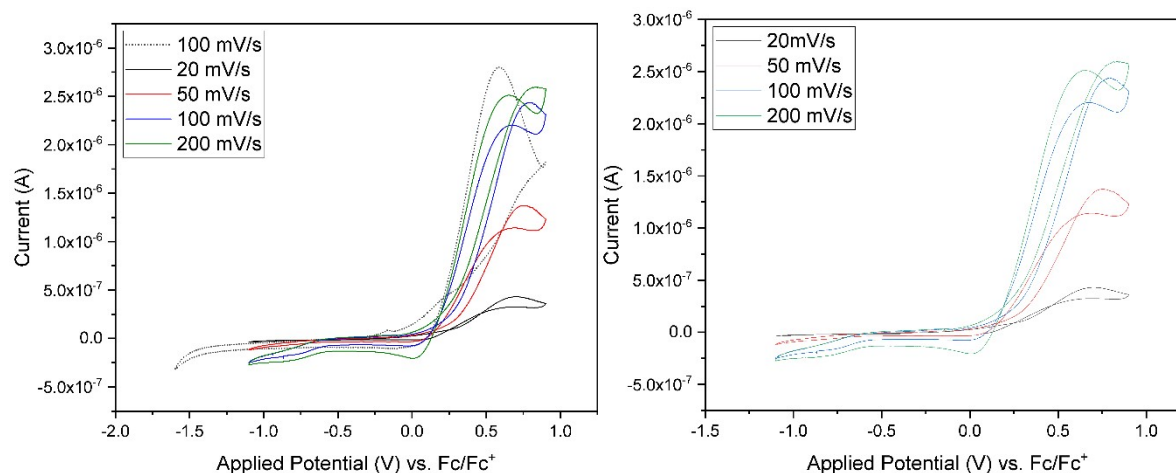


**Figure S19.** Cyclic voltammograms of **C6**  $[\text{Cu}_2(\text{L1})](\text{SbF}_6)_2$  in DCM (0.5 mM) with TBAPF<sub>6</sub>.

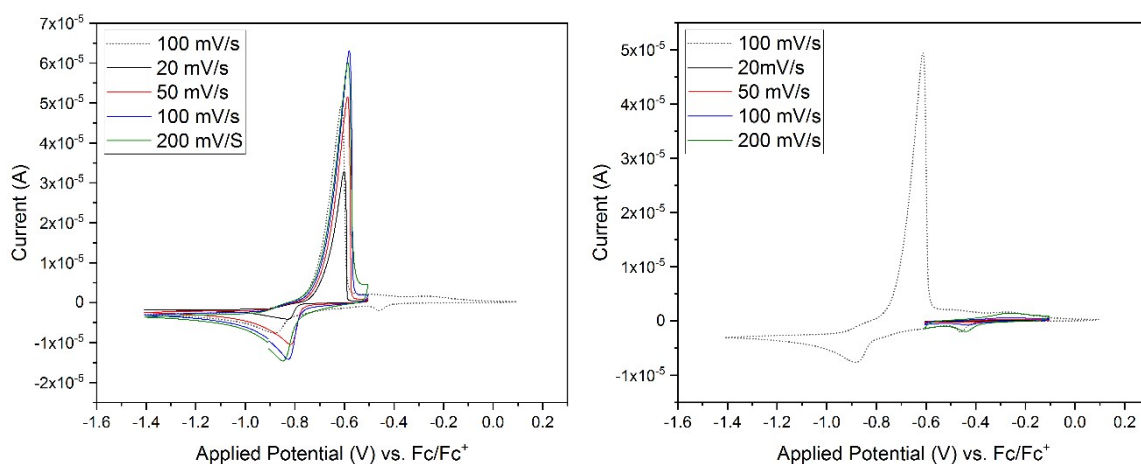


**Figure S20.** Cyclic voltammograms of **C4** ( $[\text{Cu}_2(\text{L1})(\text{MeCN})_2](\text{PF}_6)_2$ ) in MeCN (0.5 mM) with  $\text{TBAPF}_6$  at different scan rates).

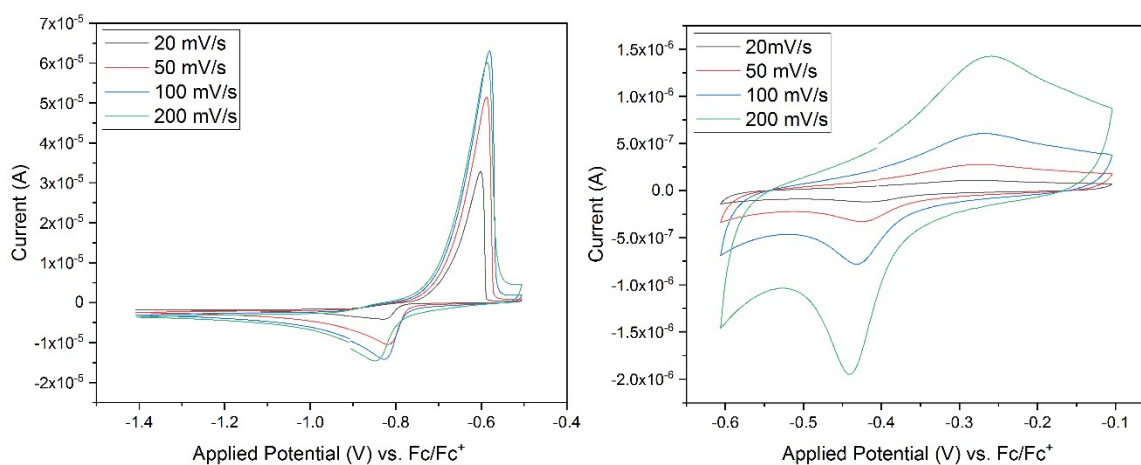


**Figure S21.** Cyclic voltammograms of **C4** ( $[\text{Cu}_2(\text{L1})(\text{MeCN})_2](\text{PF}_6)_2$ ) in MeCN (0.5 mM) with  $\text{TBAPF}_6$  at different scan rates).

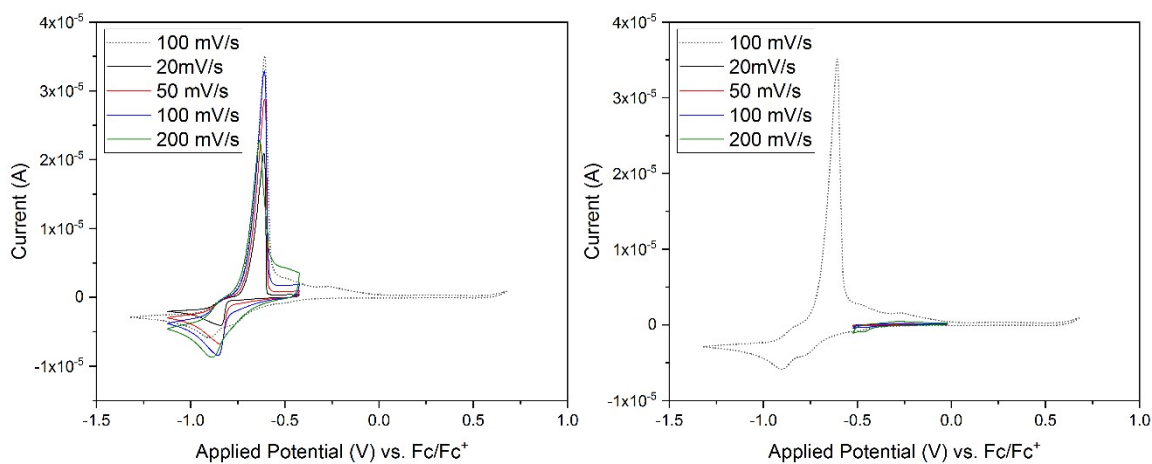


**Figure S22.** Cyclic voltammograms of **C5** ( $[\text{Cu}_2(\text{L1})(\text{MeCN})_2](\text{OTf})_2$ ) in MeCN (0.5 mM) with  $\text{TBAPF}_6$  at different scan rates).

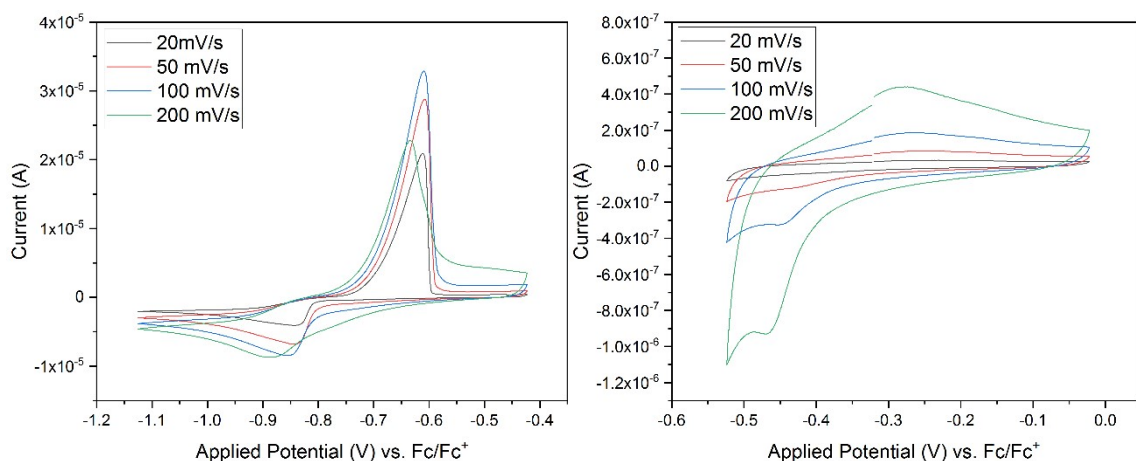


**Figure S23.** Cyclic voltammograms of **C5** ( $[\text{Cu}_2(\text{L1})(\text{MeCN})_2](\text{OTf})_2$ ) in MeCN (0.5 mM) with TBAPF<sub>6</sub> at different scan rates.

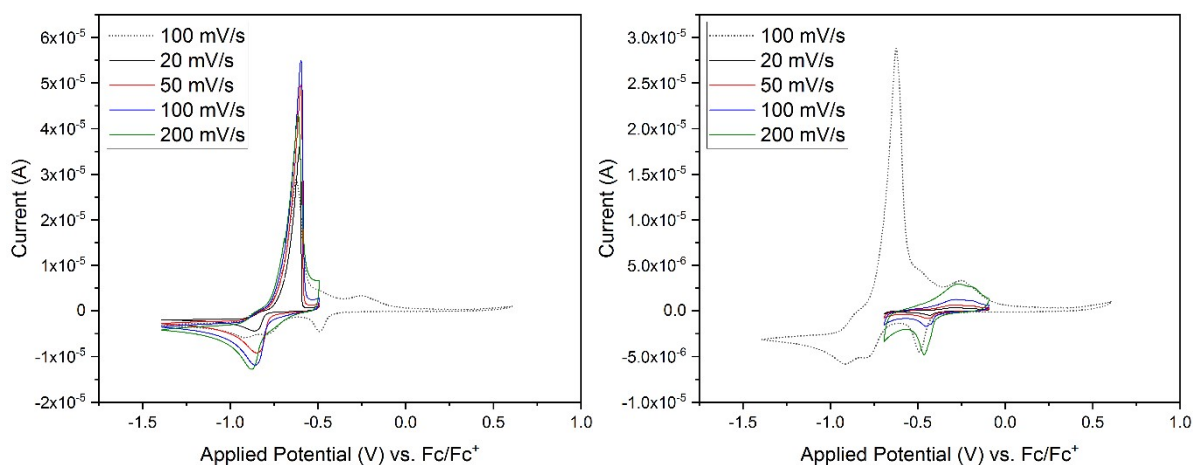


**Figure S24.** Cyclic voltammograms of **C7** ( $[\text{Cu}(\text{L3})(\text{MeCN})]\text{PF}_6$ ) in MeCN (0.5 mM) with TBAPF<sub>6</sub> at different scan rates.

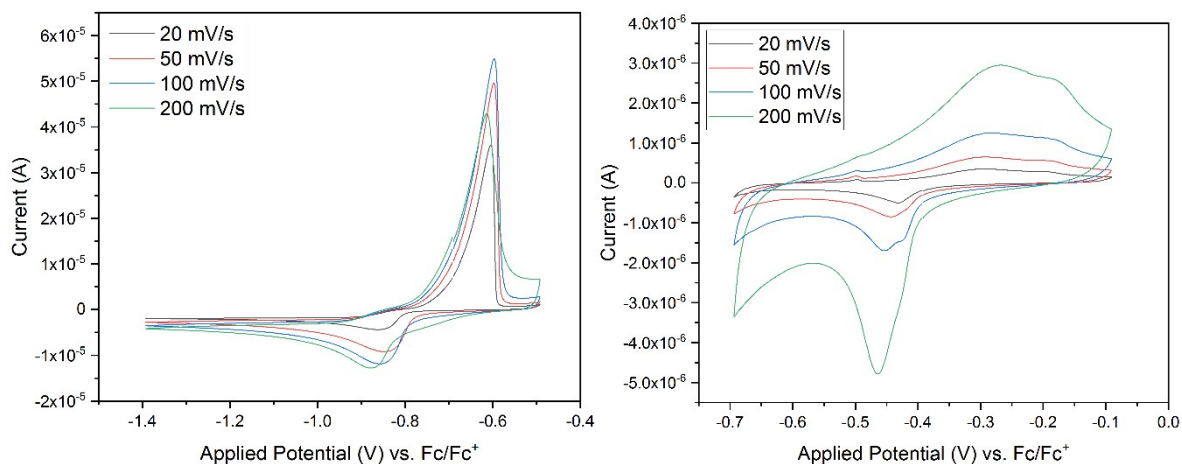


**Figure S25.** Cyclic voltammograms of **C7** ( $[\text{Cu}(\text{L3})(\text{MeCN})]\text{PF}_6$ ) in MeCN (0.5 mM) with TBAPF<sub>6</sub> at different scan rates.

The combined cyclic voltammograms at different scan rates of **P** (Figure S26) indicate an irreversible redox behavior of the peroxido complex. Furthermore, decomposition at slow feed rates can be observed. Therefore, it was not possible to calculate  $E_{1/2}$ .

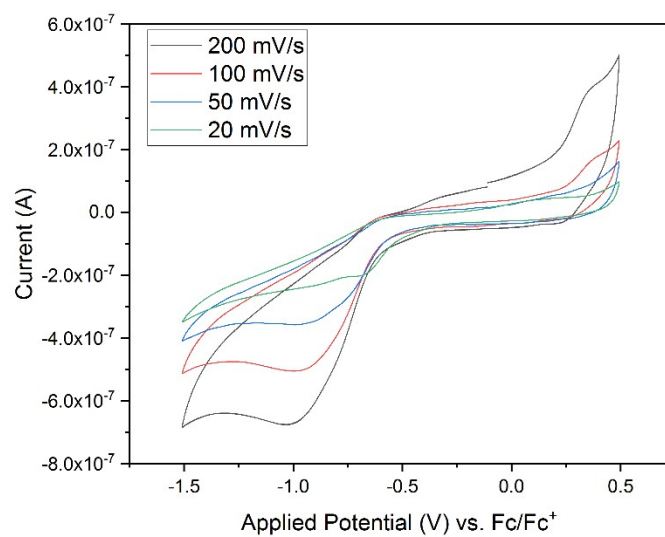
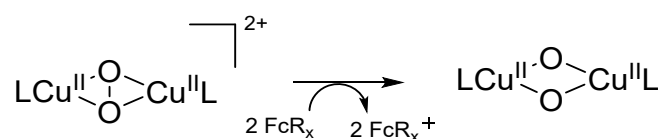


**Figure S26.** Cyclic voltammograms of the peroxido complex **P** (0.9 mM in DCM) at different scan rates starting from [L1Cu<sub>2</sub>O<sub>2</sub>](SbF<sub>2</sub>)<sub>2</sub> (potential vs Fc/Fc<sup>+</sup>).

## Spectrophotometric Titrations of **P**

### Titration of **P** with decamethylferrocene

As shown above the cyclic voltammograms of **P** indicate an irreversible behaviour. Accordingly, it was not possible to determine the redox potential of **P**. Therefore, titrations with different ferrocene derivatives which exhibit a decreasing redox potential in dependence of the alkyl substituents ( $E_{1/2}(\text{FcMe}_2) = -0.12 \text{ V vs. Fc/Fc}^+$ ,  $E_{1/2}(\text{Fc}(t\text{Bu})_4) = -0.25 \text{ V vs. Fc/Fc}^+$ ,  $E_{1/2}(\text{FcMe}_8) = -0.45 \text{ V vs. Fc/Fc}^+$ ,  $E_{1/2}(\text{Fc}^*) = -0.55 \text{ V vs. Fc/Fc}^+$ ) were performed (see Scheme S1).



**Scheme S1.** Spectroscopic titration of **P** with ferrocene derivatives ( $\text{Fc}^*$  (decamethylferrocene)  $\text{FcMe}_8$  (octamethylferrocene),  $\text{Fc}(t\text{Bu})_4$  (tetra-*tert*-butylferrocene),  $\text{FcMe}_2$  (dimethylferrocene)).

**P** (0.5 mM) was synthesized according to protocol described in the experimental part. Excess of  $\text{O}_2$  was removed by three cycles of evacuation and purging  $\text{N}_2$  at  $-80^\circ\text{C}$ . A solution of the ferrocene derivative (0.042 mmol, 4.0 eq.) in dry, degassed (3 times freeze-pump-thaw) DCM (2 mL) was prepared. For the titration the solution was cooled to  $-80^\circ\text{C}$  and the  $\text{FcR}_x$  solution was added in 0.2 eq. steps (0.05 mL of the stock solution) respectively 0.4 eq. steps (0.1 mL). The UV/Vis spectrum was recorded after stabilization of the optical spectrum. The appropriate UV/Vis spectra can be found in Figure S27 - Figure S30.

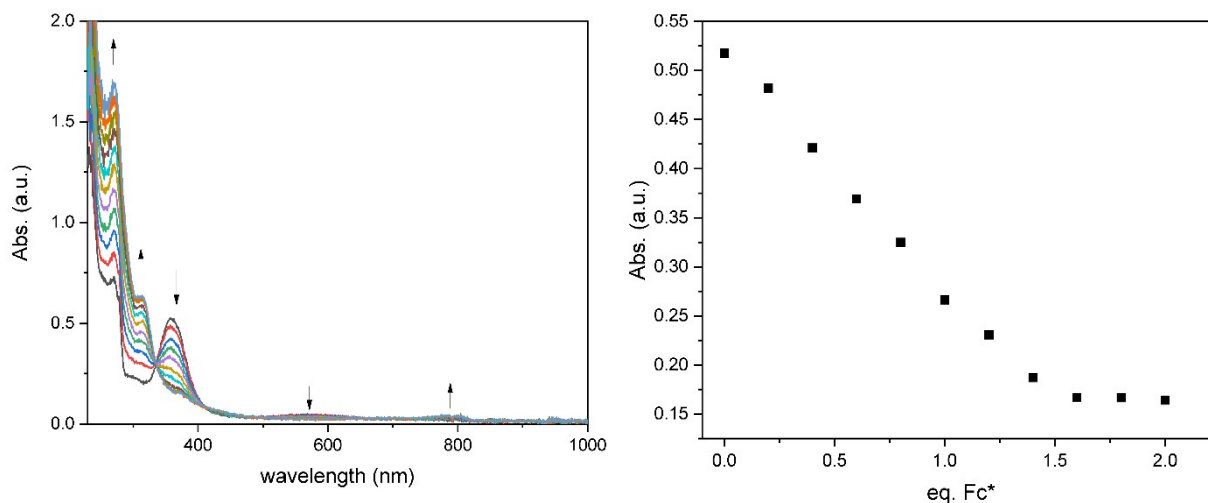


**Figure S27.** Titration of  $[\text{P}](\text{SbF}_6)_2$  (0.5 mM in DCM) with decamethylferrocene at  $-80^\circ\text{C}$  (0 to 2.0 eq.). Left: Combined UV/Vis spectra, right: Absorbance of  $[\text{P}](\text{SbF}_6)_2$  at 360 nm during the titration.

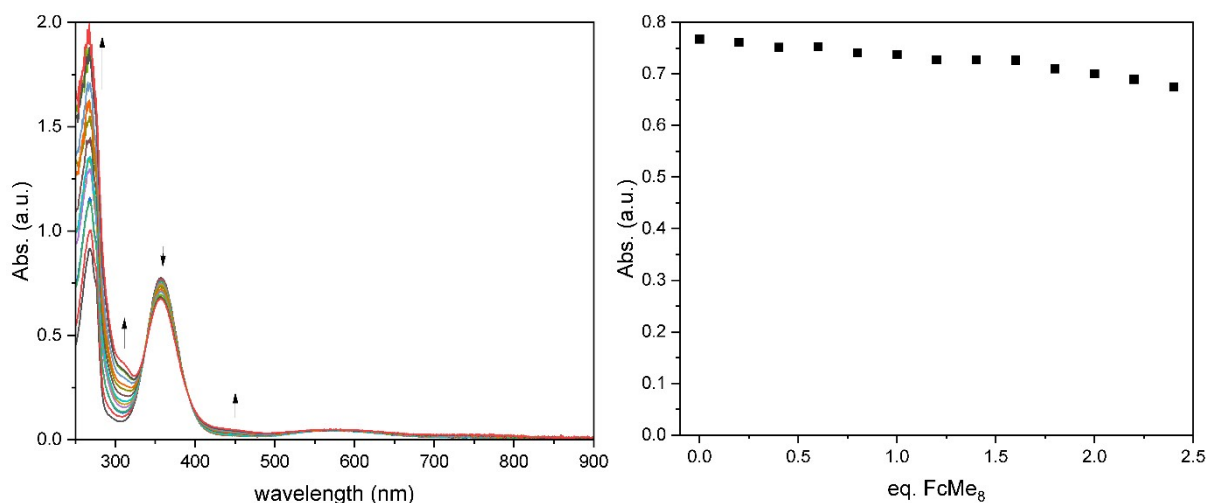


**Figure S28.** Combined UV/Vis spectra of the spectroscopic titration of [P](SbF<sub>6</sub>)<sub>2</sub> (0.5 mM in DCM) with octamethylferrocene at -80 °C.

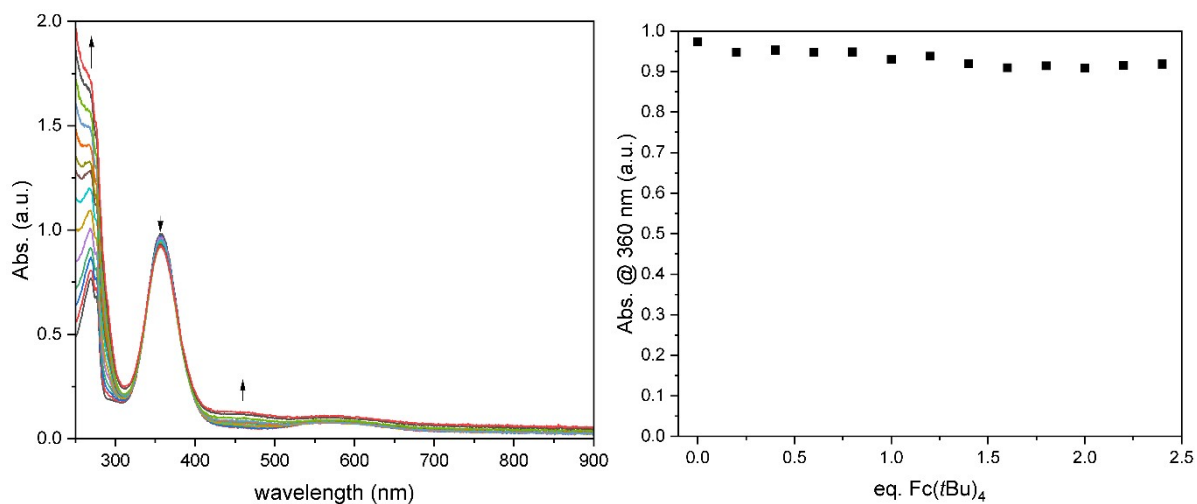


**Figure S29.** Combined UV/Vis spectra of the spectroscopic titration of [P](SbF<sub>6</sub>)<sub>2</sub> (0.5 mM in DCM) with tetra-*tert*-butylferrocene at -80 °C.

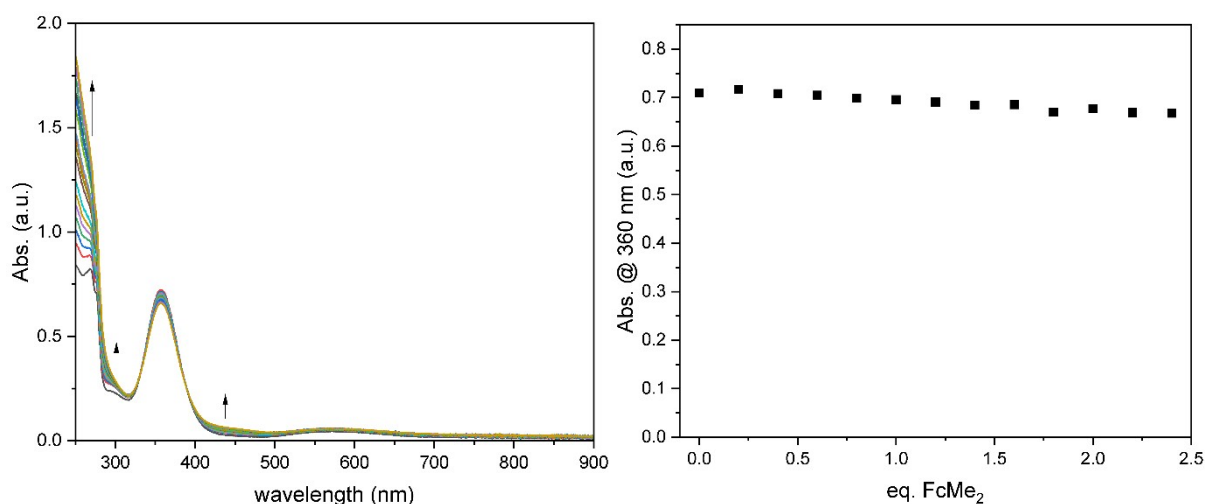


**Figure S30.** Combined UV/Vis spectra of the spectroscopic titration of [P](SbF<sub>6</sub>)<sub>2</sub> (0.5 mM in DCM) with dimethylferrocene at -80 °C.

## Kinetics

Conversion of **P** with different concentrations of  $\text{Fc}^*$  at different temperatures was monitored via UV/Vis spectroscopy. The decay of the characteristic absorption band was linearized and is depicted in Figure S31.

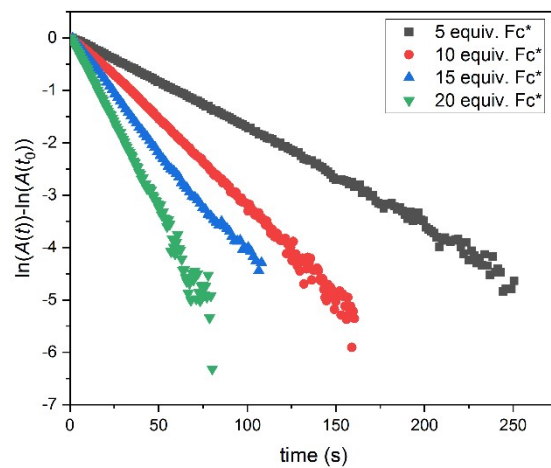


**Figure S31.** Linearized pseudo-first order plot of the reactions with **P** with 5, 10, 15 and 20 equivalents of  $\text{Fc}^*$  at  $-80\text{ }^\circ\text{C}$  in DCM. The data were obtained from stopped-flow measurements (0.5 mM).

## Iodometric experiments

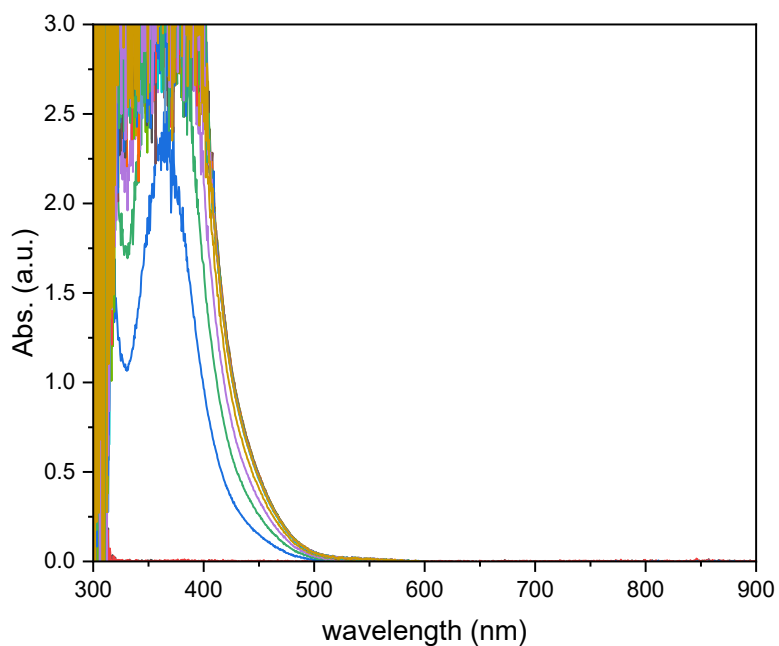


**Figure S32.** UV/Vis spectra of blind experiment: Addition of NaI to a solution containing  $\text{H}_2\text{O}_2$  and TFA (in THF).

A blind iodometric experiment was performed in THF. THF (10 mL), TFA (0.7  $\mu\text{L}$ , 1 mg,  $1 \cdot 10^{-5}$  mol, 0,04 eq. and  $\text{H}_2\text{O}_2$  (23  $\mu\text{L}$ ,  $7.7 \cdot 10^{-3}$  g,  $2.3 \cdot 10^{-4}$  mol, 1.0 eq.) were mixed and the baseline was recorded. Afterwards, NaI (30 mg,  $2.0 \cdot 10^{-4}$  mol, 0.9 eq.) in THF (0.7 mL) was added and the UV/Vis spectra displayed in Figure S33 were obtained.

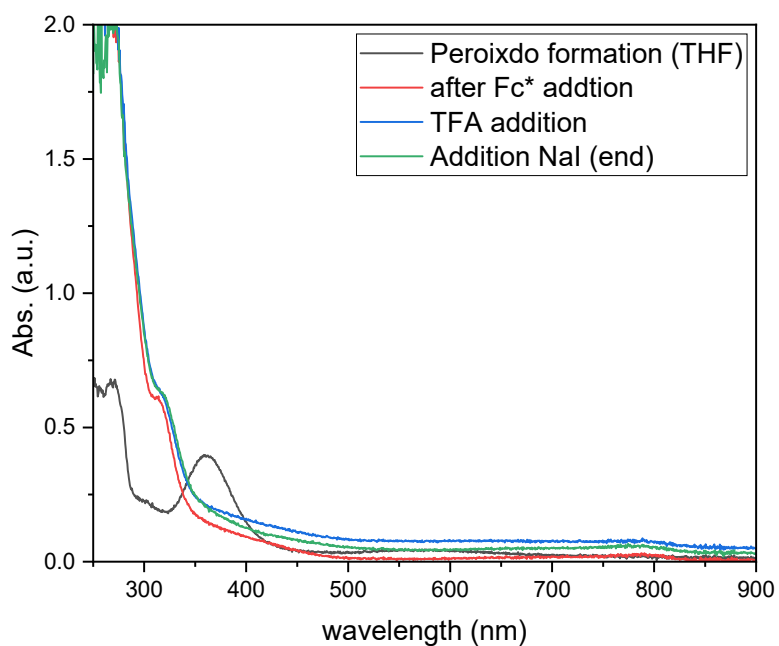


**Figure S33.** Iodometric conversion of the reduced peroxido complex in presence of TFA.

In order to determine whether  $\text{H}_2\text{O}_2$  is formed during the conversion of **P** with  $\text{Fc}^*$ , an iodometric experiment was conducted in presence of trifluoro acetic acid (TFA). **P** was synthesized (see experimental part) in THF at room temperature for 10 min and then cooled to  $-80\text{ }^\circ\text{C}$ . A stock solution of  $\text{Fc}^*$  (32.6 mg, 0.100 mmol) in THF (2 mL) was prepared. To the cold solution of **P** the stock solution of  $\text{Fc}^*$  (0.50 mL, 0.013 mol, 2.5 eq.) was added. After a reaction time of 5 min, the characteristic absorption bands of the **P** were fully decayed. TFA (0.7  $\mu\text{L}$ , 1 mg,  $1 \cdot 10^{-5}$  mol, 1 eq.) was added. After 5 min, a solution of NaI (0.35 mL of a stock solution containing 18 mg,  $1.2 \cdot 10^{-4}$  mol NaI in 3 mL THF; added amount:  $1.0 \cdot 10^{-5}$  mol, 1.0 eq.) was added. Since there was no formation of a characteristic absorption band at 365 nm (like in the blind experiment), it was assumed that no  $\text{H}_2\text{O}_2$  was formed (see Figure S33).

## Crystallographic Data

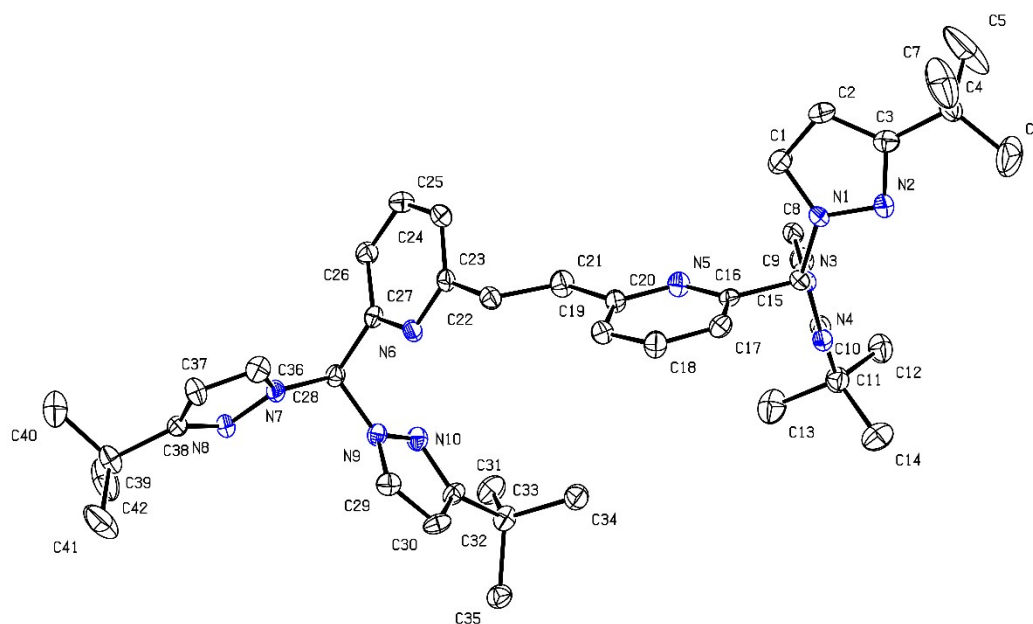


**Figure S34.** Molecular structure of the ligand **L1** in the solid state (ellipsoids drawn with 50% probability level). Hydrogen atoms were omitted for clarity.

**Table S5.** Crystal structure parameters of **L1**.

<b>L1</b>	
Empirical formula	C <sub>42</sub> H <sub>56</sub> N <sub>10</sub>
Formula weight	700.96
Temperature [K]	100
Wavelength [Å]	1.54186
Crystal system, space group	Monoclinic, Cc
a [Å]	20.621(4)
b [Å]	16.428(3)
c [Å]	11.715(2)
α [°]	90
β [°]	93.68(3)
γ [°]	90
Volume [Å <sup>3</sup> ]	3960.6(14)
Z	4
Calculated density [Mg/m <sup>3</sup> ]	1.176
Absorption coefficient [mm <sup>-1</sup> ]	0.560
F(000)	1512
Crystal size [mm]	0.140 x 0.110 x 0.100 mm
hkl range	-23<=h<=24, -19<=k<=16, -13<=l<=8
Reflections collected	10667
Independent reflections	4519
R <sub>int</sub>	0.0291
Number of parameters	481
R <sub>1</sub> [I ≥ 2σ(I)]	0.0417
wR <sub>2</sub> (all data)	0.0982
Goodness-of-fit	1.017
Largest diff. peak hole [e.Å <sup>-3</sup> ]	0.249 and -0.254

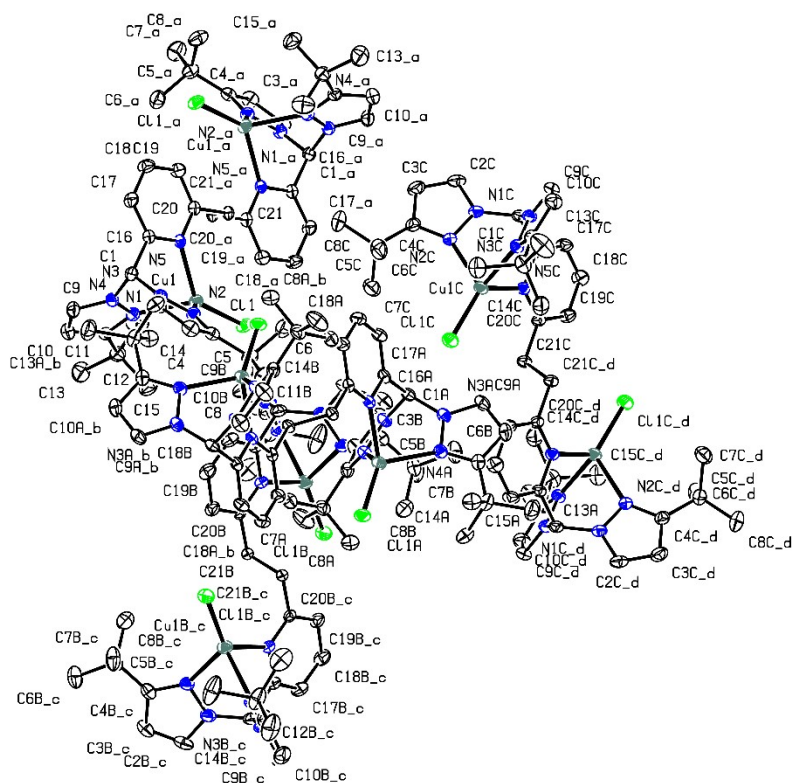


**Figure S35.** Molecular structure of **C1** in the solid state (ellipsoids drawn with 50% probability level). Hydrogen atoms were omitted for clarity.

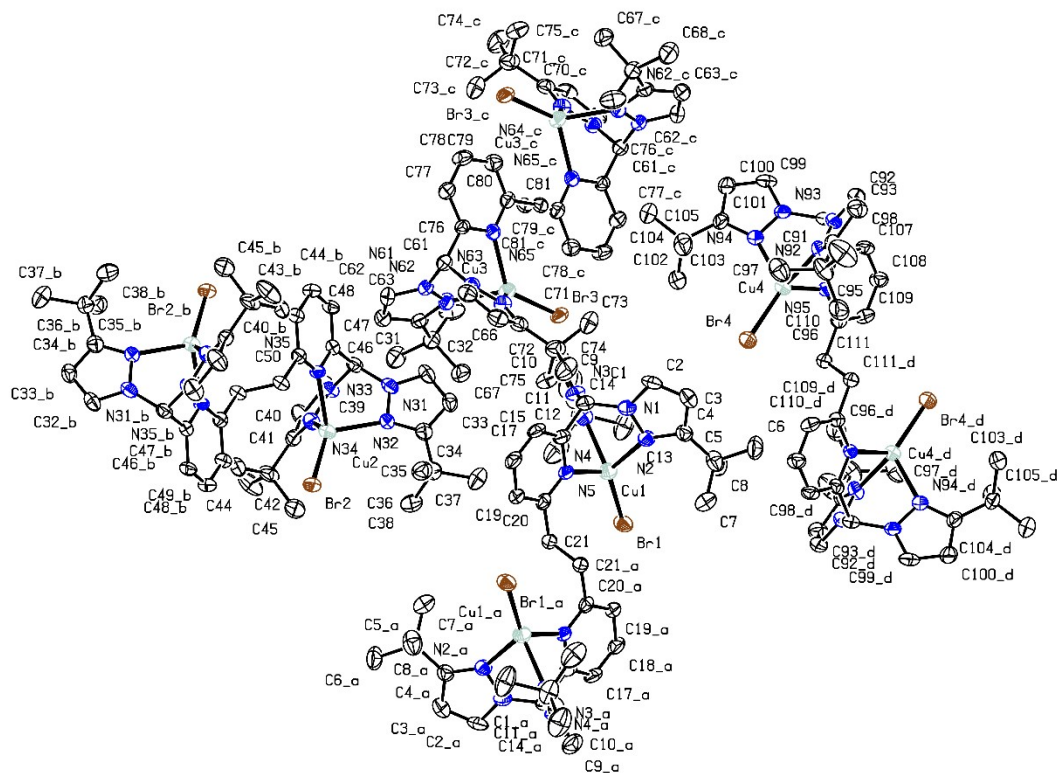


**Figure S36.** Molecular structure of **C2** in the solid state (ellipsoids drawn with 50% probability level). Hydrogen atoms were omitted for clarity.

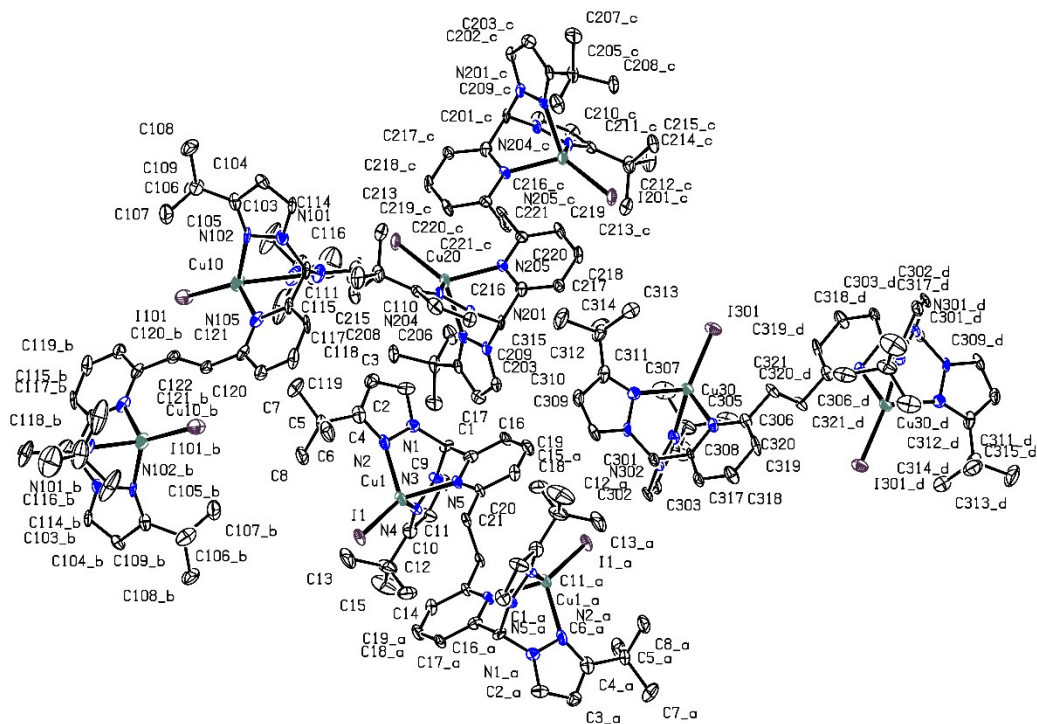


**Figure S37.** Molecular structure of **C3** in the solid state (ellipsoids drawn with 50% probability level). Hydrogen atoms were omitted for clarity.

**Table S6.** Crystal structure parameters of **C1**, **C2** and **C3**. In **C1**, **C2** and **C3** it was not possible to model the disordered solvent molecules (**C1** and **C1**: four molecules methanol in the unit cell, **C3**: four molecules CH<sub>2</sub>Cl<sub>2</sub> per unit cell) in an adequate manner, and the data set was treated with the SQUEEZE routine as implemented in PLATON<sup>15,16</sup>. **C3** is a twin and the data set was treated with the TwinRotMat routine as implemented in PLATON.<sup>15,16</sup>

	<b>C1</b> ([Cu <sub>2</sub> (L1)Cl <sub>2</sub> ])	<b>C2</b> [Cu <sub>2</sub> (L1)Br <sub>2</sub> ]	<b>C3</b> [Cu <sub>2</sub> (L1)I <sub>2</sub> ]
Empirical formula	C <sub>42</sub> H <sub>56</sub> Cl <sub>2</sub> Cu <sub>2</sub> N <sub>10</sub>	C <sub>42</sub> H <sub>56</sub> Br <sub>2</sub> Cu <sub>2</sub> N <sub>10</sub>	C <sub>42</sub> H <sub>56</sub> Cu <sub>2</sub> I <sub>2</sub> N <sub>2</sub>
Formula weight	898.94	987.86	1081.84
Temperature [K]	100	100	100
Wavelength [Å]	1.54186	0.71073 Å	0.71073
Crystal system, space group	Triclinic, <i>P</i> $\bar{1}$	Triclinic, <i>P</i> $\bar{1}$	Triclinic, <i>P</i> $\bar{1}$
a [Å]	16.007(3)	15.937(3)	15.889(14)
b [Å]	16.568(3)	16.750(3)	17.074(15)
c [Å]	16.630(3)	17.048(3)	17.838(15)
$\alpha$ [°]	89.47(3)	89.73(3)	90.35(2)
$\beta$ [°]	86.66(3)	86.39(3)	93.73(2)
$\gamma$ [°]	87.22(3)	86.79(3)	92.86(2)
Volume [Å <sup>3</sup> ]	4397.6(15)	4534.4(16)	4823(7)
Z	4	4	4
Calculated density [Mg/m <sup>3</sup> ]	1.358	1.447	1.490
Absorption coefficient [mm <sup>-1</sup> ]	2.634	2.741	2.201
F(000)	1880	2024	2186
Crystal size [mm]	0.120 x 0.100 x 0.060	0.120 x 0.090 x 0.070	0.22 x 0.16 x 0.11
hkl range	-16<=h<=18, -10<=k<=19, -19<=l<=18	-18<=h<=19, -20<=k<=19, -19<=l<=20	-18<=h<=18, -20<=k<=20, -2<=l<=20
Reflections collected	52150	76660	16413
Independent reflections	14394	16721	16413
R <sub>int</sub>	0.0232	0.0736	twin
Number of parameters	1033	1033	1034
R <sub>1</sub> [I≥2σ(I)]	0.0323	0.0645	0.0692
wR <sub>2</sub> (all data)	0.0832	0.1703	0.1889
Goodness-of-fit	1.037	0.956	1.019
Largest diff. peak hole [eÅ <sup>-3</sup> ]	0.542 and -0.470	1.669 and -0.752	3.761 and -2.517

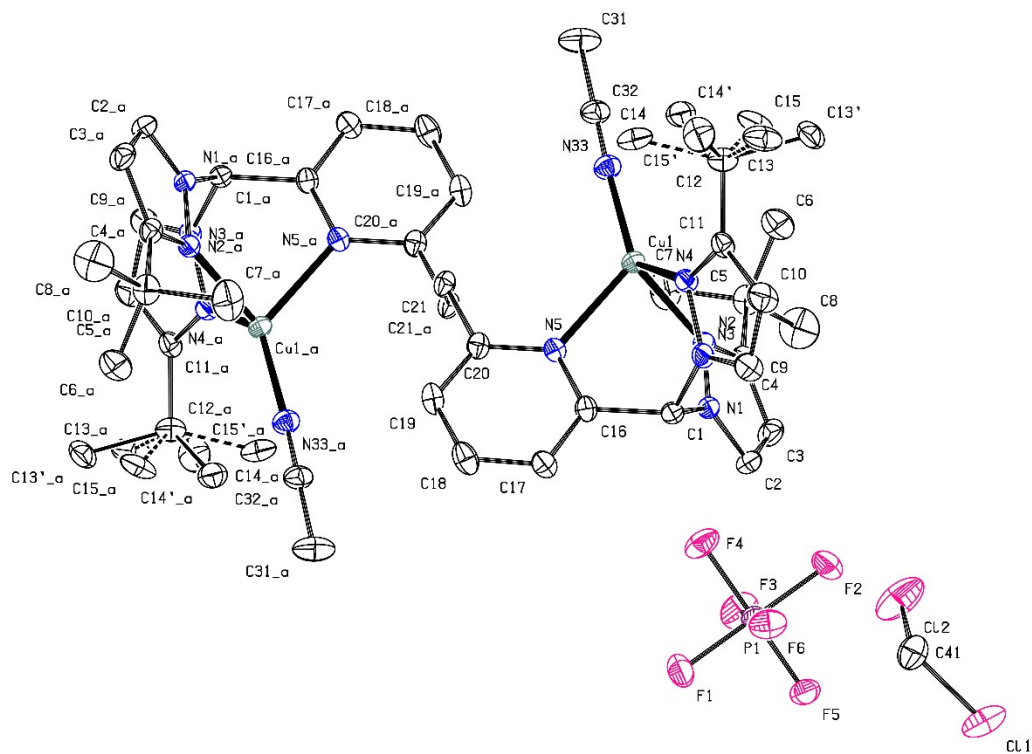


**Figure S38.** Molecular structure of **C4** in the solid state (ellipsoids drawn with 50% probability level). Hydrogen atoms were omitted for clarity.

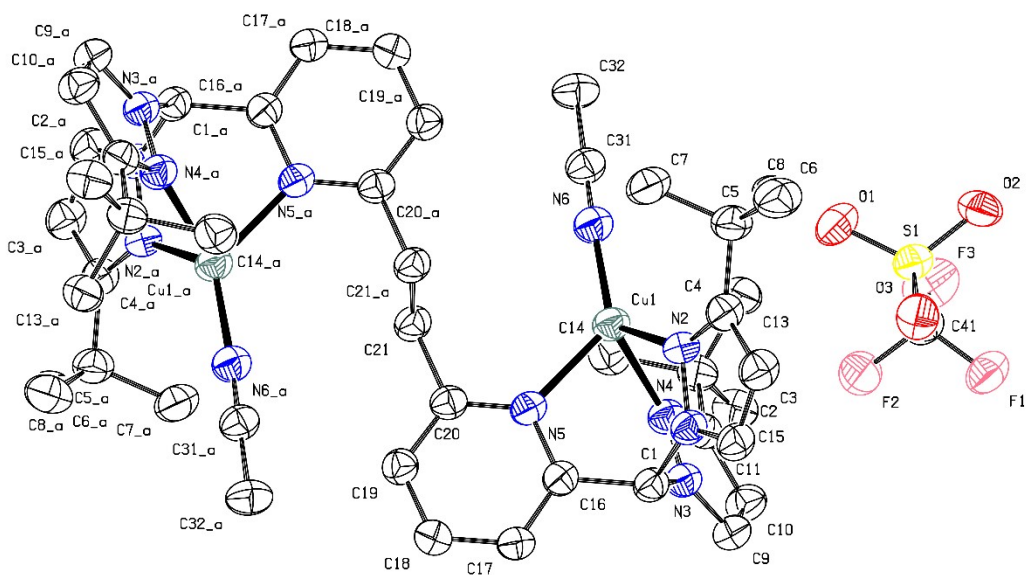


**Figure S39.** Molecular structure of **C5** in the solid state (ellipsoids drawn with 50% probability level). Hydrogen atoms were omitted for clarity.

**Table S7.** Crystal structure parameters of **C4** and **C5**.

	<b>C4</b> ([Cu <sub>2</sub> (L1)(MeCN) <sub>2</sub> ](PF <sub>6</sub> ) <sub>2</sub> )	<b>C5</b> ([Cu <sub>2</sub> (L1)(MeCN) <sub>2</sub> ](OTf) <sub>2</sub> )
Empirical formula	C <sub>48</sub> H <sub>66</sub> Cl <sub>4</sub> Cu <sub>2</sub> F <sub>12</sub> N <sub>12</sub> P <sub>2</sub>	C <sub>48</sub> H <sub>62</sub> Cu <sub>2</sub> F <sub>6</sub> N <sub>12</sub> O <sub>6</sub> S <sub>2</sub>
Formula weight	1369.94	1208.29
Temperature [K]	100	100
Wavelength [Å]	0.71073	0.71073
Crystal system, space group	Monoclinic, <i>P2<sub>1</sub>/n</i>	Monoclinic, <i>P2<sub>1</sub>/c</i>
a [Å]	11.656(2)	13.994(3)
b [Å]	15.290(3)	13.812(3)
c [Å]	17.087(3)	15.483(3)
α	90	90
β	91.29(3)	109.81(3)
γ	90	90
Volume [Å <sup>3</sup> ]	3044.5(11)	2815.7(11)
Z	2	2
Calculated density [Mg/m <sup>3</sup> ]	1.494	1.425
Absorption coefficient [mm <sup>-1</sup> ]	1.008	0.906
F(000)	1404	1252
Crystal size [mm]	0.300 x 0.250 x 0.210	0.250 x 0.200 x 0.170
hkl range	-15<=h<=14, -18<=k<=20, -22<=l<=21	-17<=h<=14, -17<=k<=17, -19<=l<=19
Reflections collected	63450	24386
Independent reflections	7359	5512
R <sub>int</sub>	0.1264	0.1096
Number of parameters	399	350
R1 [I≥2σ(I)]	0.0642	0.0637
wR2 (all data)	0.1449	0.1630
Goodness-of-fit	1.236	1.107
Largest diff. peak hole [eÅ <sup>-3</sup> ]	0.665 and -0.808	0.421 and -1.469

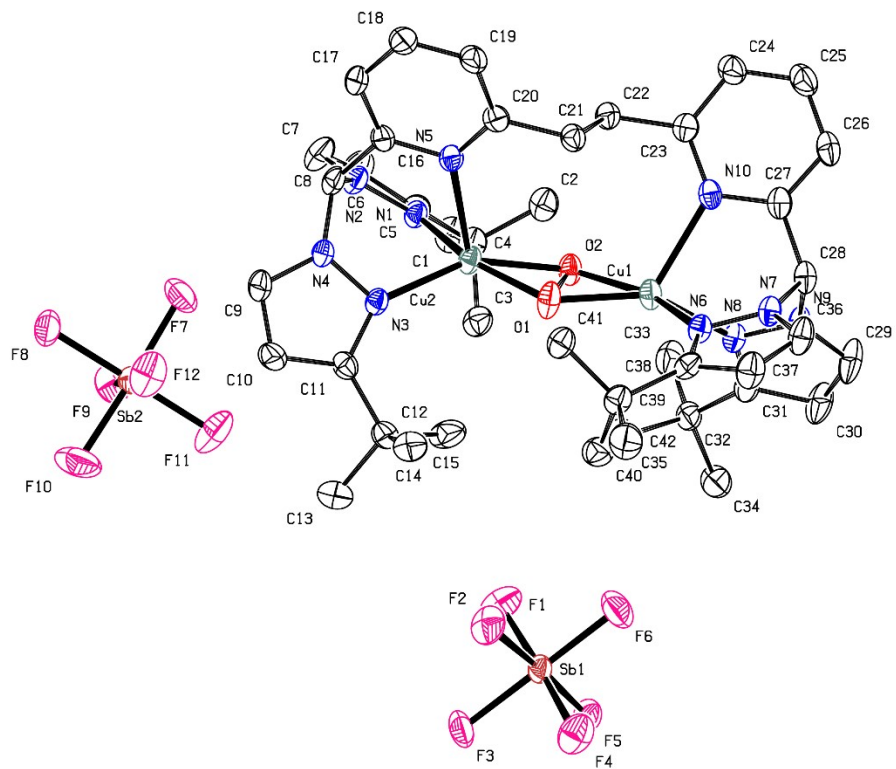


**Figure S40.** Molecular structure of **P** in the solid state (ellipsoids drawn with 50% probability level). Hydrogen atoms were omitted for clarity. 3 molecules of diethyl ether were removed via SQUEEZE.

**Table S8.** Crystal structure parameters of **P**. In **P** it was not possible to model the disordered solvent molecules (twelve molecules diethyl ether per unit cell) in an adequate manner, and the data set was treated with the SQUEEZE routine as implemented in PLATON.<sup>15,16</sup>

<b>P</b> ([Cu <sub>2</sub> O <sub>2</sub> (L1)](SbF <sub>6</sub> ) <sub>2</sub> )	
Empirical formula	C <sub>42</sub> H <sub>56</sub> Cu <sub>2</sub> F <sub>12</sub> N <sub>10</sub> O <sub>2</sub> Sb <sub>2</sub>
Formula weight	1331.54
Temperature [K]	100
Wavelength [Å]	0.71073
Crystal system, space group	Monoclinic, <i>P</i> 2 <sub>1</sub> / <i>c</i>
<i>a</i> [Å]	17.150(3)
<i>b</i> [Å]	20.445(4)
<i>c</i> [Å]	18.975(4)
$\alpha$ [°]	90
$\beta$ [°]	109.00(3)
$\gamma$ [°]	90
Volume [Å <sup>3</sup> ]	6291(2)
<i>Z</i>	4
Calculated density [Mg/m <sup>3</sup> ]	1.406
Absorption coefficient [mm <sup>-1</sup> ]	1.589
<i>F</i> (000)	2648
Crystal size [mm]	0.240 x 0.220 x 0.210
<i>hkl</i> range	-20 ≤ <i>h</i> ≤ 20, -24 ≤ <i>k</i> ≤ 23, -21 ≤ <i>l</i> ≤ 22
Reflections collected	42353
Independent reflections	11653
<i>R</i> <sub>int</sub>	0.0338
Number of parameters	643
<i>R</i> <sub>1</sub> [ <i>I</i> ≥ 2σ( <i>I</i> )]	0.0306
w <i>R</i> <sub>2</sub> (all data)	0.0792
Goodness-of-fit	1.023
Largest diff. peak hole [eÅ <sup>-3</sup> ]	0.886 and -0.366

## Key geometric parameters and energies of reduced Cu<sub>2</sub>O<sub>2</sub> species

**Table S9.** Key geometric parameters and energies of the reduced Cu<sub>2</sub>O<sub>2</sub> species with TPSSh/def2-TZVP with GD3BJ in the gas phase

	S <sup>2</sup>	Cu-Cu	O-O	Cu-N(Py)	Cu-N(Pz)	Cu-O	Energy in H	relative E in kcal/mol
red. species with peroxido-like geometry	0	3.941	1.515	2.452//2.795	1.907/2.515//1.893/2.508	1.829/2.584//1.824/2.538	-5614,38256490	22,8
red. species with peroxido-like geometry	2.01	3.577	1.484	2.090//2.090	2.102/2.153//2.102/2.153	1.996/2.046//1.996/2.046	-5614,37008190	30,6
red. species with oxido-like geometry	0	2.564	2.648	2.669//2.671	2.091/2.722//2.090/2.725	1.810/1.879/1.810/1.880	-5614,40590300	8,1
red. species with oxido-like geometry	2.00	2.802	2.522	2.661//2.661	2.144/2.220//2.144/2.220	1.880/1.890//1.880/1.890	-5614,41888470	0

## References

- 1 G. J. Kubas, B. Monzyk and A. L. Crumbliss, in *Shriver (Ed.) 1979 – Inorg. Synth.*, pp. 90–92.
- 2 H.-D. Hardt, *Z. Anorg. Allg. Chem.*, 1959, **301**, 87–96.
- 3 S. Trofimenko, J. C. Calabrese and J. S. Thompson, *Inorg. Chem.*, 1987, **26**, 1507–1514.
- 4 P. Tremouilhac, A. Nguyen, Y.-C. Huang, S. Kotov, D. S. Lütjohann, F. Hübsch, N. Jung and S. Bräse, *J. Cheminform.*, 2017, **9**, 1–13.
- 5 Chemotion, <https://chemotion.net/>, (accessed 17 November 2022).
- 6 Stoe & Cie GmbH, *X-Area LANA*, Stoe & Cie, Darmstadt, Germany, 2017.
- 7 *X-Area Integrate*, Stoe & Cie, Darmstadt, Germany, 2016.
- 8 *X-Area Recipe*, Stoe & Cie, Darmstadt, Germany, 2015.
- 9 *X-Area LANA*, Stoe & Cie, Darmstadt, Germany, 2017.
- 10 *SMART (Version 5.631)*, *SAINT (Version 8.37A)* and *SADABS (Version 2008/1)*, Bruker AXS Inc, Madison, Wisconsin, USA, 2008.
- 11 *XPREP*, Bruker AXS Inc., 2007.
- 12 G. M. Sheldrick, *Acta Crystallogr. Sect. A*, 2015, **71**, 3–8.
- 13 G. M. Sheldrick, *Acta Crystallogr. Sect. C*, 2015.
- 14 C. B. Hübschle, G. M. Sheldrick and B. Dittrich, *J. Appl. Crystallogr.*, 2011, **44**, 1281–1284.
- 15 A. L. Spek Tool, *PLATON, A Multipurpose Crystallographic Tool*, Utrecht University, The Netherlands, Utrecht 2008.
- 16 A. L. Spek, *Acta Cryst. D*, 2009, **65**, 148–155.
- 17 M. J. Frisch, G. W. Trucks, H. B. Schlegel, G. E. Scuseria, M. A. Robb, J. R. Cheeseman, G. Scalmani, V. Barone, B. Mennucci, G. A. Petersson, H. Nakatsuji, M. Caricato, X. Li, H. P. Hratchian, A. F. Izmaylov, J. Bloino, G. Zheng, J. L. Sonnenberg, M. Hada, M. Ehara, K. Toyota, R. Fukuda, J. Hasegawa, M. Ishida, T. Nakajima, Y. Honda, O. Kitao, H. Nakai, T. Vreven, J. A. Montgomery, Jr., J. E. Peralta, F. Ogliaro, M. Bearpark, J. J. Heyd, E. Brothers, K. N. Kudin, V. N. Staroverov, T. Keith, R. Kobayashi, J. Normand, K. Raghavachari, A. Rendell, J. C. Burant, S. S. Iyengar, J. Tomasi, M. Cossi, N. Rega, J. M. Millam, M. Klene, J. E. Knox, J. B. Cross, V. Bakken, C. Adamo, J. Jaramillo, R. Gomperts, R. E. Stratmann, O. Yazyev, A. J. Austin, R. Cammi, C. Pomelli, J. W. Ochterski, R. L. Martin, K. Morokuma, V. G. Zakrzewski, G. A. Voth, P. Salvador, J. J. Dannenberg, S. Dapprich, A. D. Daniels, O. Farkas, J. B. Foresman, J. V. Ortiz, J. Cioslowski, D. J. Fox, *Gaussian 09*, Wallingford CT, 2013.
- 18 M. J. Frisch, G. W. Trucks, H. B. Schlegel, G. E. Scuseria, M. A. Robb, J. R. Cheeseman, G. Scalmani, V. Barone, G. A. Petersson, H. Nakatsuji, X. Li, M. Caricato, A. V. Marenich, J. Bloino, B. G. Janesko, R. Gomperts, B. Mennucci, H. P. Hratchian, J. V. Ortiz, A. F. Izmaylov, J. L. Sonnenberg, D. Williams-Young, F. Ding, F. Lipparini, F. Egidi, J. Goings, B. Peng, A. Petrone, T. Henderson, D. Ranasinghe, V. G. Zakrzewski, J. Gao, N. Rega, G. Zheng, W. Liang, M. Hada, M. Ehara, K. Toyota, R. Fukuda, J. Hasegawa, M. Ishida, T. Nakajima, Y. Honda, O. Kitao, H. Nakai, T. Vreven, K. Throssell, J. A. Montgomery, Jr., J. E. Peralta, F. Ogliaro, M. J. Bearpark, J. J. Heyd, E. N. Brothers, K. N. Kudin, V. N. Staroverov, T. A. Keith, R. Kobayashi, J. Normand, K. Raghavachari, A. P. Rendell, J. C. Burant, S. S. Iyengar, J. Tomasi, M. Cossi, J. M. Millam, M. Klene, C. Adamo, R. Cammi, J. W. Ochterski, R. L. Martin, K. Morokuma, O. Farkas, J. B. Foresman, D. J. Fox, *Gaussian 16, Revision B.01*, Gaussian, Inc., Wallingford CT, 2016.
- 19 J. Tao, J. P. Perdew, V. N. Staroverov and G. E. Scuseria, *Phys. Rev. Lett.*, 2003, **91**, 146401.
- 20 V. N. Staroverov, G. E. Scuseria, J. Tao and J. P. Perdew, *J. Chem. Phys.*, 2003, **119**, 12129–12137.
- 21 V. N. Staroverov, G. E. Scuseria, J. Tao and J. P. Perdew, *J. Chem. Phys.*, 2004, **121**, 11507.
- 22 F. Weigend and R. Ahlrichs, *Phys. Chem. Chem. Phys.*, 2005, **7**, 3297.
- 23 K. Eichkorn, F. Weigend, O. Treutler and R. Ahlrichs, *Theor. Chem. Acc.*, 1997, **97**, 119–124.

- 24 A. Schäfer, C. Huber and R. Ahlrichs, *J. Chem. Phys.*, 1994, **100**, 5829–5835.
- 25 F. Weigend, M. Häser, H. Patzelt and R. Ahlrichs, *Chem. Phys. Lett.*, 1998, **294**, 143–152.
- 26 S. Grimme, S. Ehrlich and L. Goerigk, *J. Comput. Chem.*, 2011, **32**, 1456–1465.
- 27 L. Goerigk and S. Grimme, *Phys. Chem. Chem. Phys.*, 2011, **13**, 6670–6688.
- 28 For TPSSh, the values of the original paper have been substituted by the corrected values kindly provided by S. Grimme as private communication.
- 29 A. Hoffmann, R. Grunzke and S. Herres-Pawlis, *J. Comput. Chem.*, 2014, **35**, 1943–1950.
- 30 E. D. Glendening, C. R. Landis and F. Weinhold, *J. Comput. Chem.*, 2013, **34**, 1429–1437.
- 31 E. D. Glendening, J. K. Badenhop, A. E. Reed, J. E. Carpenter, J. A. Bohmann, C. M. Morales, P. Karafiloglou, C. R. Landis, and F. Weinhold, *NBO 7.0*, Theoretical Chemistry Institute, University of Wisconsin, Madison, USA, 2018.
- 32 F. Weinhold and C. R. Landis, *Valency and Bonding*, Cambridge University Press, 2009.
- 33 D.-P. Funeriu, *Bull. Soc. Chim.*, **133**, 673–678.
- 34 JP2017/57177, 2017.
- 35 A. Hoffmann, U. Flörke, M. Schürmann and S. Herres-Pawlis, *Eur. J. Org. Chem.*, 2010, **2010**, 4136–4144.
- 36 M. Roemer, B. W. Skelton, M. J. Piggott and G. A. Koutsantonis, *Dalton Trans.*, 2016, **45**, 18817–18821.
- 37 A. Paul, R. Borrelli, H. Bouyanfif, S. Gottis and F. Sauvage, *ACS omega*, 2019, **4**, 14780–14789.
- 38 Claudia Wilfer, Patricia Liebhäuser, Hannes Erdmann, Alexander Hoffmann and Sonja Herres-Pawlis, *Eur. J. Inorg. Chem.*, 2015, **2015**, 494–502.
- 39 Sonja Herres-Pawlis, Ulrich Herber, Katharina Hegner, Daniel Wolters and Dirk Kuckling, *Chem. Ber.*, 2016, **2017**.
- 40 A. Hoffmann, C. Citek, S. Binder, A. Goos, M. Rübhausen, O. Troeppner, I. Ivanović-Burmazović, E. C. Wasinger, T. D. P. Stack and S. Herres-Pawlis, *Angew. Chem. Int. Ed.*, 2013, **52**, 5398–5401.